

We appreciate the reviewer's comments and did our best to address them. Our response and modifications to the manuscript are appended below (*Reviewer comments in blue italic*/response in regular font):

The point about best not to do flux calculations between just two points was not made - as the authors' appear to argue about - out of concerns regarding statistical precision, but of accuracy. Even if the pore water profile only permits to use one data point, a two-point line approach is never satisfactory. It does not look to me like the authors followed the editor's simple and well meaning suggestion of a way forward.

The reviewer criticized again that we follow a two-point approach to calculate diffusive benthic fluxes across the sediment-water interface and recommends instead to interpolate between multiple points to derive the concentration gradient. We are unaware of any specific suggestions from the editor regarding the best way to proceed with this point of criticism and it is clearly not our goal to recklessly decline well-intentioned comments from reviewers or editors.

While we would love to follow the reviewer's recommendation (to add an additional point to our diffusive flux calculations) in order to get our study accepted, we cannot do this because following this approach would yield benthic flux estimates that are incorrect. We would like to explain this and defend our view with a sketch illustrating the scientific rationale behind our flux calculations (see Figure 1 below). Peru margin sediments are characterized by high iron concentrations within the surface sediments (~1 cm) but the concentrations decline shortly below because dissolved iron is precipitated with hydrogen sulfide that is generated by bacterial sulfate reduction (Scholz et al., 2011; Noffke et al., 2012). Therefore, dissolved iron is transported by diffusion both in an upward direction across the sediment-water interface and in a downward direction into the sulfidic zone of the sediments. Lumping samples from both the upward- and downward-directed concentration gradients (light and dark gray arrays in Figure 1) into one single flux calculation may be statistically desirable but is mechanistically wrong.

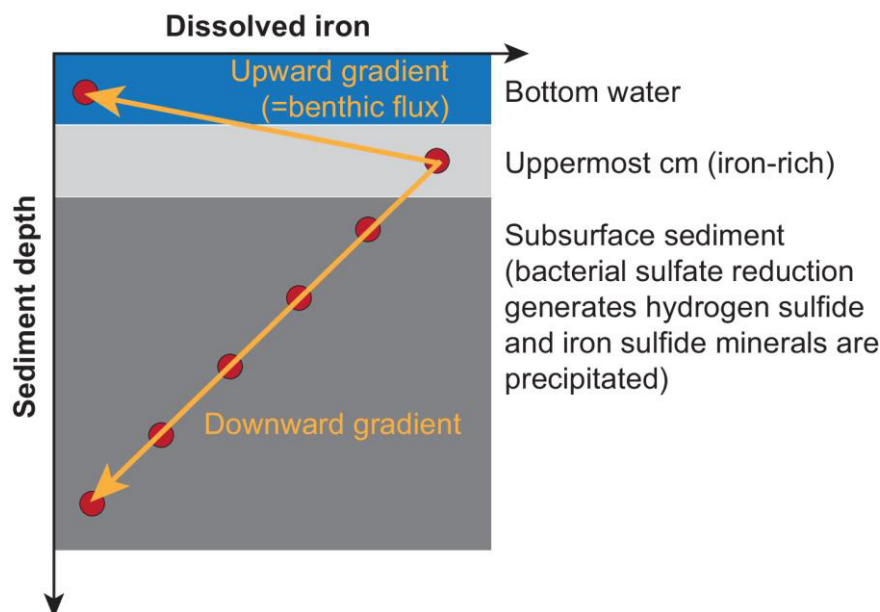


Figure 1. Sketch illustrating the scientific rationale of benthic flux calculations.

The accuracy of flux calculations based on curve-fitting exercise depends on the choice of the fitting function and the precision of the measured data. In the ideal case, a perfect fit function that considers each source and sink would pass through all the measured data points, and result in the same flux that we had calculated. Unfortunately, there is no single fitting function for dissolved iron that we are aware of. The largest uncertainty in our calculations lies not with the goodness of fit below the upper centimeters (which plays no role in the driving the Fe flux across the sediment surface) but in the resolution of the measured data close to the sediment-water interface. The only way to get a statistically better estimate of the dissolved iron flux across the sediment-water interface is to collect multiple samples within the uppermost 1 cm of the sediment. Given the fluffy character of surface sediments on the Peruvian margin, such an approach is not feasible using conventional approaches for pore water recovery. The other reviewer noted that more elaborate sampling techniques are available. That is true and we added a paragraph to the manuscript (lines 322 – 330) noting that those methods were not available during our research expedition “ Due to the coarse resolution of our pore water profiles and the steep gradients between the uppermost pore water and bottom water sample (see close-up profiles, Fig. S1 and S2 in the supplement), we chose to follow previous studies (Pakhomova et al., 2007; Noffke et al., 2012; Scholz et al., 2016, 2019; Lenstra et al., 2019) and calculate diffusive benthic fluxes based on a two point concentration gradient. Including deeper samples into a linear regression or applying more advanced curve fitting methods would reduce the statistical uncertainty but fail to capture the sharp concentration gradients at the sediment surface and thus lead to erroneous flux estimates (cf. Shibamoto and Harada, 2010).” We note, however, that those methods are typically applied in coastal research and not utilized on a routine basis on sea-going expeditions during which multiple cores are collected within a short time period. Moreover, our group (Scholz et al., 2011, 2016, 2019; Noffke et al., 2012; Dale et al., 2015) and multiple other research groups around the world (Sundby et al., 1986; Warnken et al., 2001; Pakhomova et al., 2007; Covelli et al., 2008; Shibamoto and Harada, 2010; Lenstra et al., 2019) have been following this approach of using two concentration points to calculate benthic fluxes for years demonstrating that it is widely accepted by the scientific community.

We discuss and acknowledge all the shortcomings of our approach in the manuscript and expanded on this aspect even further in the revised version. However, there is no scientifically sound alternative to this approach and we sincerely hope that we could clarify this with our letter.

Between line 393 and 396 the authors claim that the two methods of flux calculations are "largely consistent in direction and slope". I still don't see that. There is some agreement, but almost as much disagreement. Table 2 has three entries where both methods' numbers are given. Two agree in direction, one doesn't. Only one of the two is reasonably close regarding the slope, the other is a factor of two different. In Fig. 5, we have got the two matches in direction (Sta 4 and 6), but three mismatches (Sta 5 and 9 are going in opposite directions, 10 shows no flux vs outward flux; with Sta 1 I don't understand, why the benthic flux line does not go through the data). I cannot help, but to me, the claim that there "largely" is an agreement looks a bit preconceived. My conclusion is, that either the methodology is limited under the given circumstances, or there are internal dynamics in the Fe cycle that are not revealed by the study.

The reviewer correctly mentioned that there is not an agreement in direction and slope between diffusive fluxes and fluxes from benthic chamber incubations at all stations. To make clear that the agreement, between the fluxes derived from the two different methods, is in particular the case for Station 4 and 6, located inside the OMZ, we realized the following modifications to the manuscript.

Lines 20 – 24 “Diffusive Fe fluxes and Fe fluxes from benthic chamber incubations (-0.3 – -17.5 mmol $m^{-2} y^{-1}$) are broadly consistent at stations within the oxygen minimum zone, where the flux magnitude is highest, indicating that diffusion is the main transport mechanism of dissolved Fe across the sediment-water interface.”

Lines 393 – 397 “At some stations the incubation data were consistent in direction and slope with the diffusive fluxes. In particular at Station 4 and 6 inside the OMZ, where the highest diffusive fluxes of -17.5 and -8.0 mmol $m^{-2} y^{-1}$ were observed, expected and observed concentration gradients were in good agreement”

Lines 440 – 444 “Consistent with this notion, the slope calculated from benthic diffusive fluxes is in good agreement with the concentration gradients observed within the benthic chambers at two stations within the OMZ (Station 4 and 6) (Fig. 5). Moreover, our fluxes from benthic chamber incubations and diffusive fluxes are of similar magnitude at these stations (Table 2).”

Regarding the reviewer’s concerns that either the methodology is limited or that there are internal dynamics in the Fe cycle, that are not revealed by our study, leading to the variations between the two flux estimates we can refer to chapter 4.1.1 in our manuscript. In this chapter we discuss different aspects that can exert an important control on the benthic Fe cycle, in particular during benthic chamber incubation, and that can modify Fe fluxes and thus leading to variations between the two flux estimates. Further, in lines 447 – 451 we mention that scatter in data from benthic chamber incubations is a common observation “Some of the concentration gradients in benthic chambers are non-linear, indicating that the Fe flux was not constant during the incubations. This is a common observation in Fe flux data from benthic chamber incubations and higher Fe fluxes generally have higher R^2 values for the linear regressions (Friedrich et al., 2002; Turetta et al., 2005; Severmann et al., 2010; Lenstra et al., 2019).” This may be a potential limitation of the method when fluxes are low and lead to mismatches between different flux estimates (Station 1, 9 and 10). However, the similarity of benthic fluxes within the oxygen minimum zone (Station 4 and 6) still supports our conclusion, that diffusion is the main transport mechanisms of dissolved Fe from pore water into incubated bottom water. At the same time, the agreement in flux magnitude between the two different methods, also suggests that our diffusive flux estimates from a two-point concentration gradient are correct.

References

- Covelli, S., Faganeli, J., De Vittor, C., Predonzani, S., Acquavita, A. and Horvat, M.: Benthic fluxes of mercury species in a lagoon environment (Grado Lagoon, Northern Adriatic Sea, Italy), *Appl. Geochemistry*, 23(3), 529–546, doi:10.1016/j.apgeochem.2007.12.011, 2008.
- Dale, A. W., Nickelsen, L., Scholz, F., Hensen, C., Oschlies, A. and Wallmann, K.: A revised global estimate of dissolved iron fluxes from marine sediments, *Global Biogeochem. Cycles*, 29(5), 691–707, doi:10.1002/2014GB005017, 2015.
- Friedrich, J., Dinkel, C., Friedl, G., Pimenov, N., Wijsman, J., Gomoiu, M.-T., Cociasu, A., Popa, L. and Wehrli, B.: Benthic Nutrient Cycling and Diagenetic Pathways in the North-western Black Sea, *Estuar. Coast. Shelf Sci.*, 54(3), 369–383, doi:10.1006/ecss.2000.0653, 2002.
- Lenstra, W. K., Hermans, M., Séguret, M. J. M., Witbaard, R., Behrends, T., Dijkstra, N., van Helmond, N. A. G. M., Kraal, P., Laan, P., Rijkenberg, M. J. A., Severmann, S., Teacă, A. and Slomp, C. P.: The shelf-to-basin iron shuttle in the Black Sea revisited, *Chem. Geol.*, 511(April), 314–341, doi:10.1016/j.chemgeo.2018.10.024, 2019.

- Noffke, A., Hensen, C., Sommer, S., Scholz, F., Bohlen, L., Mosch, T., Graco, M. and Wallmann, K.: Benthic iron and phosphorus fluxes across the Peruvian oxygen minimum zone, *Limnol. Oceanogr.*, 57(3), 851–867, doi:10.4319/lo.2012.57.3.0851, 2012.
- Pakhomova, S. V., Hall, P. O. J., Kononets, M. Y., Rozanov, A. G., Tengberg, A. and Vershinin, A. V.: Fluxes of iron and manganese across the sediment–water interface under various redox conditions, *Mar. Chem.*, 107(3), 319–331, doi:10.1016/j.marchem.2007.06.001, 2007.
- Scholz, F., Hensen, C., Noffke, A., Rohde, A., Liebetrau, V. and Wallmann, K.: Early diagenesis of redox-sensitive trace metals in the Peru upwelling area - response to ENSO-related oxygen fluctuations in the water column, *Geochim. Cosmochim. Acta*, 75(22), 7257–7276, doi:10.1016/j.gca.2011.08.007, 2011.
- Scholz, F., Löscher, C. R., Fiskal, A., Sommer, S., Hensen, C., Lomnitz, U., Wuttig, K., Göttlicher, J., Kossel, E., Steininger, R. and Canfield, D. E.: Nitrate-dependent iron oxidation limits iron transport in anoxic ocean regions, *Earth Planet. Sci. Lett.*, 454, 272–281, doi:10.1016/j.epsl.2016.09.025, 2016.
- Scholz, F., Schmidt, M., Hensen, C., Eroglu, S., Geilert, S., Gutjahr, M. and Liebetrau, V.: Shelf-to-basin iron shuttle in the Guaymas Basin, Gulf of California, *Geochim. Cosmochim. Acta*, 261, 76–92, doi:10.1016/j.gca.2019.07.006, 2019.
- Severmann, S., McManus, J., Berelson, W. M. and Hammond, D. E.: The continental shelf benthic iron flux and its isotope composition, *Geochim. Cosmochim. Acta*, 74(14), 3984–4004, doi:10.1016/j.gca.2010.04.022, 2010.
- Shibamoto, Y. and Harada, K.: Silicon flux and distribution of biogenic silica in deep-sea sediments in the western North Pacific Ocean, *Deep Sea Res. Part I Oceanogr. Res. Pap.*, 57(2), 163–174, doi:10.1016/j.dsr.2009.10.009, 2010.
- Sundby, B., Anderson, L. G., Hall, P. O. J., Iverfeldt, Å., van der Loeff, M. M. R. and Westerlund, S. F. G.: The effect of oxygen on release and uptake of cobalt, manganese, iron and phosphate at the sediment-water interface, *Geochim. Cosmochim. Acta*, 50(6), 1281–1288, doi:10.1016/0016-7037(86)90411-4, 1986.
- Turetta, C., Capodaglio, G., Cairns, W., Rabar, S. and Cescon, P.: Benthic fluxes of trace metals in the lagoon of Venice, *Microchem. J.*, 79(1–2), 149–158, doi:10.1016/j.microc.2004.06.003, 2005.
- Warnken, K. W., Gill, G. A., Griffin, L. L. and Santschi, P. H.: Sediment-water exchange of mn, fe, ni and zn in galveston bay, texas, *Mar. Chem.*, 73(3–4), 215–231, doi:10.1016/S0304-4203(00)00108-0, 2001.

1 **The control of hydrogen sulfide on benthic iron and**
2 **cadmium fluxes in the oxygen minimum zone off Peru**

3

4 Anna Plass^{1*}, Christian Schlosser¹, Stefan Sommer¹, Andrew W. Dale¹, Eric P.
5 Achterberg¹, Florian Scholz^{1*}

6 ¹GEOMAR Helmholtz Centre for Ocean Research Kiel, Wischhofstraße 1-3, 24148
7 Kiel, Germany

8 *Correspondence to: Anna Plass (aplass@geomar.de), Florian Scholz
9 (fscholz@geomar.de)

10

11 **Abstract**

12 Sediments in oxygen-depleted marine environments can be an important sink or
13 source of bio-essential trace metals in the ocean. However, the key mechanisms
14 controlling the release from or burial of trace metals in sediments are not exactly
15 understood. Here, we investigate the benthic biogeochemical cycling of Fe and Cd in
16 the oxygen minimum zone off Peru. We combine bottom water and pore water
17 concentrations, as well as benthic fluxes determined from pore water profiles and in-
18 situ from benthic chamber incubations, along a depth transect at 12° S. In agreement
19 with previous studies, both concentration-depth profiles and in-situ benthic fluxes
20 indicate a release of Fe from sediments to the bottom water. Diffusive Fe fluxes and
21 Fe fluxes from benthic chamber incubations ($-0.3 - -17.5 \text{ mmol m}^{-2} \text{ y}^{-1}$) are broadly
22 consistent at ~~most~~ stations within the oxygen minimum zone, where the flux magnitude
23 is highest, indicating that diffusion is the main transport mechanism of dissolved Fe
24 across the sediment-water interface. The occurrence of mats of sulfur oxidizing
25 bacteria on the seafloor represents an important control on the spatial distribution of
26 Fe fluxes by regulating hydrogen sulfide (H_2S) concentrations and, potentially, Fe
27 sulfide precipitation within the surface sediment. Rapid removal of dissolved Fe after
28 its release to anoxic bottom waters hints to oxidative removal by nitrite and interactions
29 with particles in the near-bottom water column. Benthic flux estimates of Cd suggest a
30 flux into the sediment within the oxygen minimum zone. Fluxes from benthic chamber
31 incubations (up to $22.6 \text{ } \mu\text{mol m}^{-2} \text{ y}^{-1}$) exceed diffusive fluxes ($< 1 \text{ } \mu\text{mol m}^{-2} \text{ y}^{-1}$) by a
32 factor > 25 , indicating that downward diffusion of Cd across the sediment-water
33 interface is of subordinate importance for Cd removal from benthic chambers. As Cd
34 removal in benthic chambers co-varies with H_2S concentrations in the pore water of
35 surface sediments, we argue that Cd removal is mediated by precipitation of CdS within
36 the chamber water or directly at the sediment-water interface. A mass balance
37 approach, taking into account the contributions of diffusive and chamber fluxes as well
38 as Cd delivery with organic material, suggests that CdS precipitation in the near-bottom
39 water could make an important contribution to the overall Cd mass accumulation in the
40 sediment solid phase. According to our results, the solubility of trace metal sulfide
41 minerals ($\text{Cd} \ll \text{Fe}$) is a key-factor controlling trace metal removal and consequently
42 the magnitude as well as the temporal and spatial heterogeneity of sedimentary fluxes.
43 We argue that depending on their sulfide solubility, sedimentary source or sink fluxes
44 of trace metals will change differentially as a result of declining oxygen concentrations

45 and an associated expansion of sulfidic surface sediments. Such a trend could cause
46 a change in the trace metal stoichiometry of upwelling water masses with potential
47 consequences for marine ecosystems in the surface ocean.

48

49

50 **1. Introduction**

51

52 **1.1 Scientific rationale**

53 The world's oceans are losing oxygen (e.g. Keeling et al. 2010; Stramma et al.
54 2010; Helm et al. 2011). In total around 2 % of oxygen has been lost over the past five
55 decades (Schmidtko et al., 2017) and an expansion of oxygen minimum zones (OMZs)
56 in the tropical oceans has been documented over the same timespan (Stramma et al.,
57 2008). The biogeochemical cycling of several nutrient-type trace metals (TMs) is likely
58 to be particularly susceptible to changing oxygen concentrations as they occur in
59 different oxidation states (e.g. Fe, Mn, Co) and/or are ~~precipitated~~precipitate as sulfide
60 mineral in anoxic-sulfidic environments (e.g. Fe, Zn, Cd; listed in the order of
61 decreasing sulfide solubility). However, with the exception of Fe (Dale et al., 2015a;
62 Lohan and Bruland, 2008; Rapp et al., 2018; Schlosser et al., 2018; Scholz et al.,
63 2014a), little information is available on how other TM fluxes will respond to ocean
64 deoxygenation. As certain TMs are essential for the growth of marine organisms (e.g.
65 Fe, Mn, Co, Ni, Zn, Cd), TM availability can (co-)limit primary productivity and therefore
66 affect oceanic carbon sequestration through the biological pump (Saito et al., 2008;
67 Moore et al., 2013; Morel et al., 2014). As a consequence, a better understanding of
68 how TMs respond to low oxygen conditions is essential for predicting how marine
69 ecosystems and the carbon cycle will evolve in the future ocean, with modelling
70 scenarios predicting a continuation of ocean deoxygenation (Bopp et al., 2002;
71 Oschlies et al., 2008; Keeling et al., 2010)

72 Marine sediments are an important source or sink of TMs to the ocean under
73 low oxygen conditions (Böning et al., 2004; Brumsack, 2006; Scor Working Group,
74 2007; Severmann et al., 2010; Noble et al., 2012; Biller and Bruland, 2013; Conway
75 and John, 2015b; Klar et al., 2018). In the OMZ off the coast of Peru, substantial fluxes

76 of reduced Fe and other TMs across the sediment-bottom water interface have been
77 documented (Noffke et al., 2012; Scholz et al., 2016) or inferred (Hawco et al., 2016).
78 While a number of studies have addressed biogeochemical processes that lead to
79 benthic Fe release, the key biogeochemical processes and conditions that control the
80 sedimentary release or burial of other TMs in open marine systems are still poorly
81 constrained. Moreover, a detailed picture of removal or stabilization processes and
82 rates that take place in the highly dynamic water layer overlying the seafloor is lacking.

83 In this article, we compare the benthic biogeochemical cycling of Fe and Cd. It
84 has been established that the Peruvian OMZ represents a source of dissolved Fe to
85 the ocean (Noffke et al., 2012; Fitzsimmons et al., 2016; John et al., 2018). In contrast,
86 earlier studies have demonstrated that OMZs represent a sink for Cd (Janssen et al.,
87 2014; Böning et al., 2004). Because of their contrasting tendency to form sulfide
88 minerals and different supply pathways to the sediment, Fe and Cd can serve as
89 prototypes to provide information about how sedimentary fluxes of different TMs may
90 respond to declining oxygen concentrations. Under more reducing conditions the
91 mobility of TMs can either be enhanced or diminished, e.g., through precipitation of
92 sulfide minerals that are buried in the sediments (e.g. Westerlund et al., 1986; Rigaud
93 et al., 2013; Olson et al., 2017). Increased burial or release of TMs at the seafloor can
94 have an impact on the amplitude of primary productivity, especially at the eastern
95 ocean boundaries where the near-bottom water column is connected to the surface
96 ocean via upwelling. Moreover, since the inventories of TMs in the ocean are generally
97 dependent on the respective input and output fluxes, changes in the balance between
98 trace metal recycling and burial can have an impact on oceanic TM reservoirs on longer
99 timescales. By comparing the benthic biogeochemical cycling of Fe and Cd across
100 spatial and temporal redox gradients, we aim to provide general constraints on how
101 the stoichiometry of bio-essential TMs in seawater may be affected by ocean
102 deoxygenation.

103

104 **1.2. Marine biogeochemistry of iron**

105 Iron is the most abundant TM in phytoplankton and part of a range of
106 metalloenzymes that are involved in important biological functions, such as
107 photosynthesis or nitrogen fixation (Twining and Baines, 2013). Despite Fe being
108 highly abundant in the continental crust, its low availability limits primary productivity in

109 up to 30 % of the surface ocean area (Moore et al., 2013). This limitation arises from
110 the low solubility of its thermodynamically stable form in oxic waters, Fe(III).
111 Concentrations can reach up to ~ 1 nM when Fe(III) is kept in solution through
112 complexation with organic ligands (Rue and Bruland, 1997; Liu and Millero, 2002; Boyd
113 and Ellwood, 2010; Raiswell and Canfield, 2012). The thermodynamically stable form
114 of Fe under anoxic conditions, Fe(II), is more soluble and therefore anoxic waters are
115 typically characterized by higher dissolved Fe concentrations (up to tens of nM)
116 (Conway and John, 2014; Vedamati et al., 2014; Fitzsimmons et al., 2016; Schlosser
117 et al., 2018).

118 Sediments within OMZs are considered an important source of dissolved Fe and
119 some of the highest sedimentary Fe fluxes have been observed in these regions
120 (Severmann et al., 2010; Noffke et al., 2012). Under anoxic conditions, Fe(II) can be
121 liberated from the sediments into pore waters from Fe-(oxyhydr)oxides through
122 reductive dissolution by microbes or abiotic reduction with H₂S (Canfield, 1989). In the
123 absence of oxygen, dissolved Fe(II) escapes the rapid re-oxidation and subsequent
124 (oxyhydr)oxide precipitation and can, therefore, diffuse from pore waters into bottom
125 waters. However, in anoxic OMZs, where denitrification takes place, Fe(II) can also be
126 re-oxidized with nitrate as a terminal electron acceptor, either mediated by nitrate-
127 reducing microbes or abiotically through reaction with nitrite (Straub et al., 1996;
128 Carlson et al., 2013; Scholz et al., 2016; Heller et al., 2017). The solubility of Fe in
129 sulfidic (i.e. NO₃⁻ and NO₂⁻ depleted) water is relatively high (Rickard et al., 2006) and
130 during sulfidic events dissolved Fe can accumulate in the water column (up to
131 hundreds of nM) because of decreased Fe oxidation (Scholz et al., 2016) and
132 stabilization as aqueous Fe sulfide complexes and clusters (Schlosser et al., 2018).
133 However, Fe fluxes across the benthic boundary have also been hypothesized to
134 decrease under strongly sulfidic conditions in the surface sediments, when pore waters
135 become oversaturated with respect to Fe monosulfide (Scholz et al., 2014), which is
136 the precursor for pyrite (FeS₂) (Raiswell and Canfield, 2012).

137

138 **1.3. Marine biogeochemistry of cadmium**

139 Cd is abundant in phytoplankton despite concentrations that are one order of
140 magnitude lower than Fe (Moore et al., 2013; Twining and Baines, 2013). A function
141 for Cd as a catalytic metal atom in the carbonic anhydrase protein has been found in

142 diatoms (Lane and Morel, 2000) and it can also substitute Zn and enhance
143 phytoplankton growth under Zn limitation in different phytoplankton species (Price and
144 Morel, 1990; Lee and Morel, 1995; Sunda and Huntsman, 2000; Xu et al., 2008). In
145 marine sediments Cd can be released from the solid phase to the pore waters through
146 the remineralization of organic matter (Klinkhammer et al., 1982; Collier and Edmond,
147 1984; Gendron et al., 1986; Gerringa, 1990; Audry et al., 2006; Scholz and Neumann,
148 2007). After its release to the pore water, Cd can diffuse across the sediment-water
149 interface. Under anoxic and sulfidic conditions, Cd is thought to be precipitated as CdS
150 (Greenockite) and retained in the sediment (Westerlund et al., 1986; Gobeil et al.,
151 1987; Rosenthal et al., 1995; Audry et al., 2006). Due to its low sulfide solubility, CdS
152 can precipitate at much lower H₂S concentrations than FeS (mackinawite) (Morse and
153 Luther, 1999).

154 Most previous studies have focused on the benthic cycling of Cd in near- and
155 in-shore environments such as estuaries and lagoons (e.g. Westerlund et al., 1986;
156 Colbert et al., 2001; Audry et al., 2006b; Metzger et al., 2007; Point et al., 2007; Scholz
157 and Neumann, 2007). By contrast, little is known about Cd cycling in open-marine
158 sedimentary environments, where the redox- and sediment-dynamics are different.
159 Previous studies on sedimentary Cd cycling generally concluded that the flux of organic
160 material and the presence of H₂S are the most important factors controlling the balance
161 between Cd recycling versus precipitation and burial (e.g. Westerlund et al., 1986;
162 Colbert et al., 2001; Audry et al., 2006; Metzger et al., 2007; Scholz and Neumann,
163 2007). Low oxygen regions in the ocean are considered an important sink for Cd
164 (Janssen et al., 2014; Conway and John, 2015a; Xie et al., 2019) and sediments below
165 OMZs are highly enriched in Cd (Ragueneau et al., 2000; Böning et al., 2004; Borchers
166 et al., 2005; Muñoz et al., 2012; Little et al., 2015). However, the respective
167 contributions of different Cd removal mechanisms to Cd accumulation in the sediment
168 have not been quantified.

169

170 **1.4. Study area**

171 Seasonal upwelling of nutrient-rich waters off the Peruvian coast in austral
172 winter leads to high rates of primary productivity in the photic zone (~ 300 mmol C m⁻³
173 d⁻¹) (Pennington et al., 2006). The combination of oxygen consumption through the
174 respiration of this organic matter and low oxygen concentrations in water masses that

175 supply upwelling regions, leads to the formation of one of the world's most intense
176 OMZs, with complete oxygen consumption in the OMZ core between ~ 100 m – 300 m
177 water depth (Karstensen et al., 2008; Thamdrup et al., 2012). Upon oxygen depletion,
178 NO_3^- can serve as an electron acceptor for respiration. Therefore, denitrification,
179 dissimilatory reduction of NO_3^- to ammonium (DNRA) and anaerobic ammonium
180 oxidation (anammox) with NO_2^- are important biogeochemical processes within the
181 anoxic and nitrogenous water column (Lam et al., 2009; Lam and Kuypers, 2011;
182 Dalsgaard et al., 2012). The OMZ overlying the Peruvian shelf is a temporally and
183 spatially dynamic system where biogeochemical conditions can range from fully oxic
184 to anoxic and sulfidic. Occasional shelf oxygenation events occur mostly during El Niño
185 events and are linked to the propagation of coastal trapped waves (Gutiérrez et al.,
186 2008). During such events, oxygenated water can be found on the upper slope to 200
187 m – 300 m water depth (Levin et al., 2002). By contrast, sulfidic events can occur
188 during periods of stagnation, when oxygen, NO_3^- and NO_2^- become depleted in the
189 water column due to sluggish ventilation. Once NO_3^- and NO_2^- are depleted,
190 chemolithoautotrophic H_2S oxidation is impeded. Hydrogen sulfide produced by
191 bacterial sulfate reduction in sediments can then be released to the water column
192 (Schunck et al., 2013) at rates reaching several $\text{mmol m}^{-2} \text{d}^{-1}$ (Sommer et al., 2016).

193 Our sampling campaign (cruises M136 and M137) took place in April and May
194 2017, during the decline of a coastal El Niño event. A coastal El Niño is a local
195 phenomenon that refers to reduced upwelling and increased sea surface temperatures
196 off the coasts of Peru and Ecuador, with typically heavy rainfall on land. During this
197 event in austral summer, coastal waters off Peru showed a strong positive sea surface
198 temperature anomaly of up to 2 to 4 °C (Echevin et al., 2018; Garreaud, 2018). The
199 warming is proposed to be a result of strong local alongshore wind anomalies and
200 equatorial Kelvin waves propagating towards the Peruvian coast (Echevin et al., 2018;
201 Peng et al., 2019).

202

203

204 **2. Methods**

205

206 **2.1 Sampling and sample handling**

207 In this study, data from three different types of samples were combined: (1) pore
208 waters for the determination of benthic diffusive fluxes and to study TM cycling in
209 sediments; (2) Benthic chamber incubations, to determine in-situ fluxes across the
210 sediment-water interface; (3) Bottom water concentration-depth profiles to determine
211 the fate of TMs in the particle-rich and dynamic near-bottom water column.

212 The sampling took place during RV Meteor cruises M136 and M137 in austral
213 autumn between April and May 2017. We also compared our data to benthic diffusive
214 Fe(II) fluxes from RV Meteor cruise M92 that took place in austral summer during
215 January 2013. Our sampling stations covered the entire Peruvian shelf and slope
216 across a transect at 12°S (Fig. 1) with water depths from 75 – to 950 m, thus including
217 stations above, inside and below the permanent OMZ. Our sampling of pore waters
218 and sample collection from benthic chamber incubations generally followed the
219 methodology described in Noffke et al. (2012).

220 Short sediment cores of 30 – 40 cm length were retrieved with a multiple corer
221 (MUC). Upon recovery, the cores were directly transferred into the ship's cool room
222 (4°C). The supernatant bottom water was instantly sampled and filtered through 0.2
223 µm cellulose acetate filters (Sartorius) and acidified to pH < 1 with subboiled distilled
224 HNO₃. The sediment cores were subsequently sampled in vertical sections in a glove
225 bag under Ar atmosphere to prevent any contact with oxygen. The sediment samples
226 were centrifuged to separate the pore waters from the sediment solid phase. Pore
227 waters were then filtered in another Ar-filled glove bag through 0.2 µm cellulose acetate
228 filters (Sartorius). An 8 ml aliquot was acidified to pH < 1 with subboiled distilled HNO₃
229 and stored in acid cleaned low-density polyethylene (LDPE) bottles for TM analysis.
230 Another aliquot was taken for analysis of H₂S concentrations. Additional sediment
231 subsamples were collected in pre-weighed cups for water content and porosity
232 determination as well as for Cd and organic C concentrations measurements in the
233 solid phase.

234 Benthic landers, constructed from titanium frames, containing two circular
235 benthic chambers for in-situ incubations, were deployed on the seafloor (see Sommer
236 et al. (2009) for details). After placement of the lander on the seafloor, the benthic
237 chambers (internal diameter of 28.8 cm) were partially driven into the sediment,
238 covering a sediment area of 651.4 cm². A volume between 12 – 18 l, overlying the first
239 20 – 30 cm of the seafloor, was enclosed in the chamber, depending on the insertion

240 depth of the chamber into the sediment. Prior to the incubation, the seawater contained
241 in the chamber was repeatedly replaced with ambient seawater to replace solutes and
242 flush out particles that might have been mobilized during the insertion of the chamber
243 into the sediment. Over the incubation time of around 32 hours, 8 consecutive samples
244 of 12 ml were filtered in-situ through 0.2 μm cellulose acetate filters (Sartorius) via
245 peristaltic pumps and collected in quartz glass tubes. All sampling tubes were acid
246 cleaned prior to use to guarantee a TM clean sampling. After recovery of the lander,
247 the quartz glass tubes were transferred to the laboratory and samples were stored in
248 acid cleaned LDPE bottles and acidified to $\text{pH} < 2$ with subboiled distilled HNO_3 . Other
249 samples were collected simultaneously for analysis of nitrogen species. The incubated
250 sediments within the benthic chamber were sampled after recovery of the lander and
251 pore waters were extracted to analyze H_2S concentrations for comparison with pore
252 water profiles from parallel MUCs.

253 To determine TM concentrations across the near-bottom water column, water
254 samples were collected at 0.5, 1.0, 2.0, 3.0 and 4.0 m above the seafloor using
255 sampling apparatus attached to the landers. Filter holders with 0.2 μm polyether
256 sulfone filters (Supor) were attached at the various depths and connected to sampling
257 tubes that went through peristaltic pumps into gas sampling bags (Tedlar). Sampling
258 at 3.0 m and 4.0 m above the seafloor was realized by attaching the filter holders and
259 tubing to an arm that was automatically unfolded upon placement of the lander at the
260 seafloor. The peristaltic pumps transferred the seawater from the sampling depths into
261 the sampling bags over the same time period as the lander incubations of around 32
262 hours. This resulted in an average sample volume of 1.5 l per depth. All filters, tubing
263 and sampling bags were acid cleaned prior to deployment to guarantee a TM clean
264 sampling. Directly after sample retrieval, ~~ana~~ 60 ml aliquot was stored in acid cleaned
265 LDPE bottles and acidified to $\text{pH} < 2$ for TM analysis. Another aliquot was taken for
266 analysis of silicic acid ($\text{Si}(\text{OH})_4$).

267

268 **2.2 Analytical methods**

269 Concentrations of $\text{Fe}(\text{II})$ in pore waters were measured on board directly after
270 sample retrieval by photometry using the ferrozine method (Stookey, 1970). Other
271 geochemical parameters in our different samples were also determined photometrical
272 (U-2001 Hitachi spectrometer) using standard techniques (Grasshoff et al., 1999).

273 Hydrogen sulfide concentrations were determined using the methylene blue method
274 and Si(OH)_4 concentrations were determined using a heptamolybdate solution as
275 reagent. Concentrations of nitrogen species were determined by an auto-analyzer
276 (QuAatro, SEAL Analytical) using sulfanilamide as reagent (Hydes et al., 2010).

277 For TM analysis of bottom water samples we followed the procedure described
278 by Rapp et al. (2017), whereby the TMs were pre-concentrated by a fully automated
279 device (SeaFAST). After raising the sample pH to 6.4 with an ammonium acetate buffer
280 (1.5 M), 15 ml of sample was loaded onto a chelating resin column, where the seawater
281 matrix was rinsed off, before the TMs were collected into 1ml elution acid (1 M
282 subboiled HNO_3). Due to the smaller size of pore water samples and samples from
283 benthic lander incubations, a half-automated device (Preblab) with a smaller sample
284 loop and thus dead volume was used. On this device, sample loading and collection
285 as well as the addition of buffer was done manually. For samples from benthic lander
286 incubations and pore waters, an amount of 3 ml and 1 ml, respectively, was needed
287 for pre-concentration. The samples were diluted with de-ionised water (MilliQ,
288 Millipore) to increase the sample volume to 5 ml for samples from benthic chamber
289 incubations and to 3 ml for pore waters. The pre-concentrated samples were measured
290 by ICP-MS (HR-ICP-MS; Thermo Fisher Element XR) and TM concentrations were
291 quantified by isotope dilution. The detection limits were 28.8 pM for Fe and 0.8 pM for
292 Cd (Rapp et al., 2017). Accuracies for replicate measurements of reference seawater
293 certified for TMs are listed in Table 1.

294 For the calculation of sedimentary Cd enrichments (Cd_{xs}), Cd and Al contents
295 in sediments were determined following total digestions of freeze dried and ground
296 sediment samples. The sediment was digested in 40 % HF (suprapure), 65 % HNO_3
297 (suprapure) and 60 % HClO_4 (suprapure). Concentrations were measured by ICP-OES
298 (VARIAN 720-ES). The reference standard MESS was used to check the digestion
299 procedure. The accuracy was ± 0.3 % for Cd and ± 1.3 % for Al (MESS-3 Cd: $0.24 \pm$
300 $0.01 \mu\text{g g}^{-1}$, recommended value $0.24 \pm 0.01 \mu\text{g g}^{-1}$, MESS-3 Al: $8.59 \pm 0.11 \mu\text{g g}^{-1}$,
301 recommended value $8.59 \pm 0.23 \mu\text{g g}^{-1}$).

302 Organic carbon content in the sediment was determined using an Elemental
303 Analyzer (Euro EA) after removal of inorganic carbon with 0.25 mM HCl. Precision of
304 the measurement was ± 1 %.

305

337 2.3 Diffusive flux calculations

338 Benthic diffusive fluxes (F_D) were determined using Fick's first law of diffusion
339 using concentration gradients between the uppermost pore water sample (0 – 1 cm)
340 and the overlying bottom water (dC/dx) (Boudreau, 1997):

$$341 F_D = -\Phi D_{sed}(dC/dx) \quad (1)$$

342 The effective molecular diffusion coefficients of Fe and Cd for sediments (D_{sed}) were
343 calculated from the molecular diffusion coefficient in seawater (D_{sw}) under standard
344 conditions (Li and Gregory, 1974) by adjusting it to in-situ temperature, pressure and
345 salinity applying the Stokes-Einstein Equation. We determined the diffusion
346 coefficients for sediments as follows:

$$347 D_{sed} = D_{sw}/\theta^2 \quad (2)$$

348 Tortuosity (θ) was calculated from porosity (Φ) as follows (Boudreau, 1997):

$$349 \theta^2 = 1 - \ln(\phi^2) \quad (3)$$

350 Positive values represent a flux from the bottom water into the sediment pore
351 water, negative values a flux from the sediment pore water into the bottom water. All
352 input values for the diffusive flux calculations are listed in Tables S1 and S2 in the
353 supplement.

354 Due to the coarse resolution of our pore water profiles and the steep gradients
355 between the uppermost pore water and bottom water sample (see close-up profiles,
356 Fig. S1 and S2 in the supplement), we chose to follow previous studies (~~e.g. Noffke et~~
357 ~~al., 2012; Lenstra et al., 2019; Scholz et al., 2019~~)(~~Pakhomova et al., 2007; Noffke et~~
358 ~~al., 2012; Scholz et al., 2016, 2019; Lenstra et al., 2019~~) and calculate diffusive benthic
359 fluxes based on a two point concentration gradient. Including deeper samples into a
360 linear regression or applying more advanced curve fitting methods would reduce the
361 statistical uncertainty, but fail to capture the sharp concentration gradients at the
362 sediment surface, and thus, leading lead to erroneous flux estimates (cf. Shibamoto
363 and Harada, 2010).

364 The fluxes from benthic lander incubations were calculated by fitting a linear
365 regression to the concentration change over time. The relevant equations are listed
366 together with the coefficients of determination (R^2) in Table S4 in the supplement.
367 Concentration changes over time were converted to fluxes by taking into account the

368 water volume enclosed in the benthic chamber, estimated for each deployment from
369 the insertion depth of the benthic chamber into the sediment. The uncertainties of
370 fluxes were estimated by propagating the uncertainties of the linear regressions.
371 Following previous studies (e.g. Friedrich et al. (2002); Lenstra et al. (2019)), only
372 fluxes where the linear regression has an $R^2 > 0.3$ are reported in Tables 2 and 3.

373

374

375 **3. Results**

376

377 **3.1 Biogeochemical conditions in the water column**

378 Due to the particular atmospheric and oceanographic conditions, the decline of
379 a coastal El Niño during our sampling campaign (cruises M136 and M137), the water
380 column overlying the Peruvian shelf was oxygenated. Oxygen concentrations were >
381 20 μM in the water column down to around 100 m water depth. However, bottom water
382 oxygen concentrations directly above the seafloor, measured using optodes attached
383 to lander, were below the detection limit (> 1 μM) at the shallowest station (Station 1).
384 The OMZ, with O_2 concentrations < 5 μM , extended from around 120 to 400 m water
385 depth. The water column within the OMZ was nitrogenous (i.e. NO_3^- reducing) as
386 indicated by the presence of NO_2^- ($\geq 4 \mu\text{M}$), an intermediate product of denitrification
387 (Zumft, 1997). Oxygen gradually increased to > 50 μM below 400 m towards 950 m
388 water depth (Fig. 2). As we will compare some of our data to those of an earlier cruise
389 (M92), the corresponding oxygen distribution across the Peruvian continental margin
390 is shown for comparison (Fig. 2).

391

392 **3.2 Bottom water, pore water and benthic flux data**

393

394 **3.2.1 Iron**

395 Iron concentrations in near-bottom waters decreased from near-shore to off-
396 shore stations, from > 100 nM at the shallowest shelf station at 75 m water depth
397 (Station 1) to 6 nM at 750 m water depth (Station 9) (Fig. 3). At a number of stations

398 within the OMZ (~~Stations~~Station 3 and 4), vertical concentration gradients were
399 observed. Here Fe concentrations decreased by 15 – 20 nM from 0.5 to 4 m above the
400 seafloor. Multiple sampling at the shallowest shelf station (Station 1) revealed that Fe
401 concentrations were temporally variable and ranged from ~ 100 nM at the end of April
402 to < 60 nM at the end of May 2017.

403 Concentrations of Fe(II) in pore waters were highest (up to a few μM) in the
404 upper 5 – 10 cm of the sediment cores. Deeper in the sediment cores, concentrations
405 decreased to > 0.2 μM (Fig. 4). At all stations, sharp concentration gradients between
406 the uppermost pore water and bottom water sample were observed, with higher
407 concentrations in pore waters at the sediment surface (μM) than in the overlying bottom
408 water (nM). This observation implies a diffusive flux from pore waters into bottom
409 waters. The steepest concentration gradients across the sediment-water interface
410 were observed within the OMZ. The highest Fe(II) concentrations at the sediment
411 surface (> 6 μM) were observed at Station 4 (145 m water depth). At this station, the
412 benthic diffusive flux into the bottom waters was also highest at $-17.5 \text{ mmol m}^{-2} \text{ y}^{-1}$.
413 The lowest diffusive fluxes of 0.0 (due to concentrations below the detection limit) and
414 $-0.3 \text{ mmol m}^{-2} \text{ y}^{-1}$ were observed on the upper slope below the OMZ at Stations 9 and
415 10 respectively (Table 2). An accumulation of H_2S in pore waters coincided with a
416 depletion of Fe(II) concentrations (Fig. 4). At Station 1, we observed the highest H_2S
417 concentrations throughout the core and in particular at the sediment surface, with
418 maximum concentrations reaching > 4 mM. At Stations below the OMZ
419 (~~Stations~~Station 9 and 10), no H_2S was detected within pore waters (Fig. 4).

420 Iron concentrations inside the benthic chambers reached maximum
421 values > 300 nM. At ~~Stations~~Station 4 and 6, located inside the OMZ, concentrations
422 in the chambers increased in a linear way during the incubation. At stations above and
423 below the OMZ, we did not observe a similar trend over time. For comparison with
424 diffusive fluxes, we estimated benthic Fe fluxes from linear regressions of Fe
425 concentrations versus time (Table 2). We also calculated the theoretical concentration
426 gradients over time in the benthic chambers based on our diffusive flux estimates (Fig.
427 5). ~~The~~At some stations the incubation data were largely consistent in direction and
428 slope with the diffusive fluxes. In particular, ~~the projected and observed concentration~~
429 ~~gradients were in good agreement~~ at stationsStation 4 and 6 inside the OMZ (~~Station~~
430 ~~4 and 6~~), where the highest diffusive fluxes of -17.5 and $-8.0 \text{ mmol m}^{-2} \text{ y}^{-1}$ were

431 observed, expected and observed concentration gradients were in good agreement.
432 At these stations also the highest R^2 for the linear regressions of the concentration
433 change over the incubation time were calculated (Station 4: $R^2 = 0.7$, Station 6: $R^2 =$
434 0.5) (Table S4). At stations below the OMZ, diffusive fluxes of $< 1 \text{ mmol m}^{-2} \text{ y}^{-1}$ were
435 too low to be detected over the incubation time of 32 hours.

436

437 3.2.2 Cadmium

438 In near-bottom waters Cd concentrations increased with distance from the
439 coast, from 0.4 nM at the shallowest station at 75 m water depth (Station 1) to 1.1 nM
440 below the OMZ at 750 m water depth (Station 9). Cadmium concentrations were
441 constant at each station between 0.5 and 4 m above the seafloor (Fig. 3).

442 Cadmium concentrations in pore waters ranged between 0.1 – 2 nM (Fig. 6).
443 Within the OMZ, bottom water concentrations were higher than concentrations in pore
444 water at the sediment surface (0 - 1 cm), indicating a downward diffusive flux into the
445 sediments. The benthic diffusive fluxes inside the OMZ were on the order of 0.6 – 0.8
446 $\mu\text{mol m}^{-2} \text{ y}^{-1}$ (Table 3). In contrast, at Stations 1 and 9 an upward-directed
447 concentration gradient was observed, indicating a diffusive flux from the sediments into
448 bottom waters. The upward diffusive flux was $-1.9 \mu\text{mol m}^{-2} \text{ y}^{-1}$ above the permanent
449 OMZ and $-0.2 \mu\text{mol m}^{-2} \text{ y}^{-1}$ below the OMZ (Table 3). Pore water Cd concentrations at
450 greater sediment depths were mostly higher than bottom water concentrations. In
451 some cases (StationsStation 3 and 4), elevated pore water Cd concentrations (up to 2
452 nM) coincided with elevated H_2S concentrations (few hundred μM).

453 In the benthic chambers three different Cd trends were observed (Fig. 7). Above
454 the permanent OMZ (Station 1), Cd concentrations in the chambers were low (< 0.2
455 nM) throughout the incubation period, indicating no Cd flux. At sites within the OMZ
456 (StationsStation 4, 5 and 6), concentrations decreased from $\sim 0.6 - 0.3$ nM over the
457 course of the incubation. Below the OMZ (Stations 9 and 10), Cd concentrations in the
458 chamber were high (~ 1 nM) and remained constant or increased slightly during the
459 incubation. At sites within the OMZ, Cd removal within the chamber was near-linear
460 (StationsStation 4, 5 and 6: $R^2 = \geq 0.9$) (Table S4), which translates to a removal flux
461 of $13 - 23 \mu\text{mol m}^{-2} \text{ y}^{-1}$. The Cd removal fluxes in benthic chambers were more than

462 one order of magnitude higher than diffusive benthic fluxes ($0.6 - 0.8 \mu\text{mol m}^{-2} \text{y}^{-1}$)
463 (Table 3).

464

465

466 4. Discussion

467

468 4.1 Benthic iron cycling

469 4.1.1 Comparison of diffusive and in-situ benthic chamber iron fluxes

470 Concentrations of Fe in bottom waters from benthic chamber incubations are
471 mostly higher than in ambient bottom waters because of Fe release from the sediment
472 and an accumulation in the enclosed water volume inside the benthic chamber. In the
473 absence of oxygen and, thus, bottom-dwelling macrofauna at stations within the OMZ,
474 bioturbation and bioirrigation are unlikely to exert an important control on sedimentary
475 Fe release. Consistent with this notion, the slope calculated from benthic diffusive
476 fluxes is ~~largely consistent in good agreement~~ with the concentration gradients
477 observed within the benthic chambers (~~Fig. at two stations within the OMZ (Station 4~~
478 ~~and 6) (Fig. 5)~~). Moreover, our fluxes from benthic chamber incubations and diffusive
479 fluxes are ~~generally of the same order of of similar~~ magnitude ~~at these stations~~ (Table
480 2). Therefore, diffusive transport of dissolved Fe from the sediment into the bottom
481 water seems to be the main control on the concentration evolution observed within the
482 benthic chamber.

483 Some of the concentration gradients in benthic chambers are non-linear,
484 indicating that the Fe flux was not constant during the incubations. This is a common
485 observation in Fe flux data from benthic chamber incubations and higher Fe fluxes
486 generally have higher R^2 values for the linear regressions (Friedrich et al., 2002;
487 Turetta et al., 2005; Severmann et al., 2010; Lenstra et al., 2019). However, the non-
488 linearity can be used to identify additional processes affecting Fe concentrations and
489 fluxes within the benthic chamber, which may also affect fluxes under natural
490 conditions. One possible process that can remove dissolved Fe(II) under anoxic
491 conditions is Fe oxidation with NO_3^- as the terminal electron acceptor or oxidation with
492 NO_2^- (Straub et al., 1996; Carlson et al., 2013; Klueglein and Kappler, 2013). The

493 oxidation of reduced Fe in the absence of oxygen, either microbially mediated with
494 NO_3^- or abiotically with NO_2^- , has been hypothesized to be important in the water
495 column of the Peruvian OMZ (Scholz et al., 2016; Heller et al., 2017). During our
496 incubation at Station 4 (Fig. 8), we observed a decline in Fe concentrations during the
497 first ten hours of the incubation time. Concurrently, NO_3^- concentrations were
498 decreasing, while NO_2^- accumulated, presumably due to progressive denitrification and
499 release from the sediments. Once NO_3^- and NO_2^- were depleted, Fe concentrations
500 started to rise again, resulting in the highest in-situ Fe flux observed throughout our
501 sampling campaign (Table 2). The coincidence in timing of Fe accumulation and NO_2^-
502 decrease suggest that depletion of Fe at the beginning of the incubation was most
503 likely caused by Fe oxidation with NO_2^- . The incubation at Station 4 was the only one
504 where NO_3^- and NO_2^- were substantially removed during the incubation. However, the
505 high Fe flux cannot be interpreted as a natural flux estimate at steady state. In general,
506 we argue that bottom water NO_2^- concentrations exert a first order control on the
507 intensity of Fe efflux at the absence of oxygen and, therefore, need to be considered
508 in the evaluation of sedimentary Fe mobility in anoxic-nitrogenous OMZs.

509 During the incubations at ~~Stations~~Station 1, 9 and 10, Fe concentrations did not
510 continuously increase but fluctuated between high and low values. This observation
511 could be explained by a combination of bioirrigation and bioturbation at stations where
512 oxygen was present (~~stations~~Station 9 and 10), as well as rapid Fe oxidation and
513 precipitation processes. Under oxic conditions, bottom-dwelling macrofauna is likely to
514 increase the transfer of dissolved Fe from the sediments into the bottom water (Elrod
515 et al., 2004; Lenstra et al., 2019). During episodes of oxygenation a population of
516 macrofauna that can enhance bioturbation and bioirrigation was observed on the
517 Peruvian shelf (Gutiérrez et al., 2008). However, under oxic conditions, any Fe
518 delivered to the chamber is prone to rapid oxidative removal. Moreover, ex-situ
519 experiments have demonstrated a fast and efficient removal of up to 90% of dissolved
520 Fe in incubated bottom waters due to particle resuspension (Homoky et al., 2012).
521 Bioturbation and bioirrigation could also contribute to particle resuspension at oxic
522 stations, thus leading to removal of dissolved Fe.

523 Furthermore, colloidal Fe could modify Fe concentrations within our samples
524 and explain some of the fluctuations observed during the incubations. Colloids are
525 quite reactive, ~~they are~~ and much more soluble than larger particles ~~and~~. Therefore,

526 they can be rapidly reduced and dissolved in anoxic environments, but they can also
527 aggregate into larger particles (Raiswell and Canfield, 2012). The transfer of Fe
528 between dissolved, colloidal and particulate pools is likely to affect the balance
529 between Fe transport and re-precipitation and -deposition to some extent. However,
530 since we did not differentiate between colloidal and truly dissolved fractions during our
531 sampling, we cannot discuss this aspect further based on our data.

532 Oxidation processes and interactions with particles can efficiently remove Fe
533 shortly after its transfer to bottom waters and this process is likely to be most intense
534 close to the seafloor where the highest particle concentrations prevail. We argue that
535 the same processes are reflected by declining Fe concentrations away from the
536 seafloor in some of the bottom water profiles (at StationsStation 3 and 4) (Fig. 3).

537

538 **4.1.2 Removal rates of dissolved iron in the near-bottom water column**

539 We observed declining Fe concentrations in the first 4 m away from the seafloor
540 at StationsStation 3 and 4, which hints at removal of dissolved Fe in the near bottom
541 waters after its release from the sediments. To differentiate between dilution with
542 ambient bottom water (by currents) from Fe removal from the dissolved phase, Fe
543 concentrations were normalized by Si(OH)₄ measured in the same samples (Fig. 3).
544 Due to opal dissolution within Peru margin sediments, Si(OH)₄ is released into bottom
545 waters (Ehlert et al., 2016). In contrast to Fe, we assume that Si(OH)₄ behaves
546 conservatively and precipitation reactions within the bottom waters are of subordinate
547 importance. The decreasing Fe to Si(OH)₄ ratios at Station 3 and 4 with distance from
548 the seafloor indicate that there is Fe removal within the near-bottom water column that
549 must be related to precipitation processes or scavenging.

550 We further constrained rates of dissolved Fe removal at stations with a
551 discernable Fe to Si(OH)₄ gradient within the first 4 m distance from the seafloor. To
552 this end, we first determined an eddy diffusion coefficient (K_y) using Si(OH)₄ fluxes
553 from benthic chamber incubations (F_{Si}) (see chapter 2.3 for methodology) and the
554 known concentration gradient of dissolved Si(OH)₄ within the bottom water (d_{Si}/d_x),
555 where x is the height above the seafloor. At the seafloor, the flux of Si(OH)₄ from the
556 sediment is equal to the flux in the water column.

557
$$F_{Si} = -K_y(d_{Si}/d_x) \quad (4)$$

558 This equation can be solved for the eddy diffusion coefficient.

559 Dissolved Fe in the bottom water (DFe) can be described by the solving the
560 diffusion-reaction equation for DFe (ignoring advection and assuming a steady-state
561 first-order consumption of dissolved Fe):

$$562 \quad DFe = C_{BW} * \exp. (-\sqrt{k_{Feox}}/\sqrt{K_y}) \quad (5)$$

563 The equation can be fitted to the measured DFe concentrations in the bottom water by
564 adjusting the Fe concentration directly above the seafloor (C_{BW}) and the Fe oxidation
565 constant (k_{Feox}). From the fitted first-order rate constant k_{Feox} , the half-life for dissolved
566 Fe in bottom waters can be calculated.

567 The half-lives of dissolved Fe in the first 4 m away from the seafloor are 2.5 min
568 and 0.3 min at ~~Stations~~Station 3 and 4, respectively (Table 4). Another study reported
569 a dissolved Fe half-life of 17 hours under nitrogenous conditions in the first 10 – 20 m
570 above the seafloor in the Peruvian OMZ (Scholz et al., 2016). Our calculations suggest
571 that Fe removal in near-bottom waters is much faster. The approach assumes that
572 $Si(OH)_4$ is transported vertically by eddy diffusion and ~~eddy diffusion and~~ oxidation
573 ~~control~~controls the half-life of Fe in the first 4 m above the seafloor. It is possible that
574 our assumption of solute transport by eddy diffusion is not correct. Alternatively,
575 decreasing Fe and $Si(OH)_4$ concentration above the seafloor could be due to super-
576 imposed water layers with different Fe and $Si(OH)_4$ concentrations but little vertical
577 exchange. In this case our calculated half-life would be an underestimation.

578 As mentioned above (chapter 4.1.1), in the absence of oxygen, removal
579 processes of dissolved Fe could be related to oxidation of dissolved Fe with NO_2^- or to
580 interactions with suspended particles, which are likely to be most abundant directly
581 above the seafloor. Further research on dissolved-particulate interactions, including
582 the role of colloidal Fe, in bottom waters is needed to better constrain how sedimentary
583 Fe fluxes are modified in the near-bottom water column.

584

585 **4.1.3 Controls on the temporal variability of benthic iron fluxes**

586 The Peruvian OMZ is known to experience high-amplitude fluctuations in
587 upwelling intensity as well as variability in bottom water oxygen, NO_3^- , NO_2^- and H_2S
588 concentrations (Pennington et al., 2006; Gutiérrez et al., 2008; Graco et al., 2017;

589 Ohde, 2018). To get an insight into how different biogeochemical conditions control
590 benthic diffusive Fe(II) fluxes, we compared the fluxes from our recent cruise with
591 fluxes from our earlier cruise M92 (Fig. 9). Cruise M92 took place in austral autumn
592 2013 following the main upwelling season and during a period of intense primary
593 productivity. Due to reduced upwelling and stable density stratification, the water
594 column on the shallow shelf was not only depleted in oxygen but also in NO_3^- and NO_2^-
595 during cruise M92 (Sommer et al., 2016). Under such conditions,
596 chemolithoautotrophic H_2S oxidation with NO_3^- or NO_2^- was impeded so that pore water
597 H_2S could be released from the sediment into the water column. As a result, the water
598 column during M92 was sulfidic between around 50 – 150 m water depth with the
599 highest H_2S concentration of 13 μM observed at 50 m depth (Fig. 2). While the
600 biogeochemical conditions on the shallow shelf were fundamentally different to those
601 during M136 and M137, below 150 m water depth the conditions were largely
602 comparable (oxygen-depleted, NO_3^- : 20 – 30 μM , NO_2^- up to 9 μM between 150 – 300
603 m). At the stations with similar biogeochemical water column conditions, the Fe(II)
604 fluxes during both sampling campaigns were remarkably similar (Fig. 9). However,
605 similar to the temporal variability of Fe concentrations in bottom waters at Station 1
606 (Fig. 3), we observed a pronounced difference in the diffusive flux magnitude on the
607 shallow shelf where the biogeochemical conditions differed between both cruises. The
608 highest diffusive flux during M92 in 2013 of $-22.7 \text{ mmol m}^{-2} \text{ y}^{-1}$ was measured at Station
609 1. By contrast, during M136/137 in 2017 we determined a much lower flux of -2.6 mmol
610 $\text{m}^{-2} \text{ y}^{-1}$ at this station. During M136 and M137 the highest flux of $-17.5 \text{ mmol m}^{-2} \text{ y}^{-1}$ was
611 measured at Station 4 at 145 m water depth.

612 Diffusive fluxes are a function of the concentration gradient between pore water
613 and bottom water (Eq. (1)). As dissolved Fe concentrations in bottom waters are
614 generally much lower (nM) compared to those observed in pore waters (μM), the flux
615 magnitude is chiefly determined by differences in pore water Fe concentrations. During
616 M92, pore waters at the sediment surface were characterized by high dissolved Fe
617 concentrations (4.8 μM in the upper pore water sample), which resulted in a steep
618 gradient and a comparably high Fe flux. Under the slightly sulfidic conditions that
619 prevailed in the water column during M92, oxidative removal of dissolved Fe(II) with
620 NO_3^- or NO_2^- was impeded (Scholz et al., 2016) and dissolved Fe(II) could be stabilized
621 as aqueous iron sulfide (Schlosser et al., 2018). Therefore, the bottom water was

622 characterized by high dissolved Fe concentrations (up to 0.7 μM in the supernatant
623 bottom water of MUCs).

624 Despite oxic conditions in the water column during M136 and M137, we
625 observed much higher H_2S concentrations in surface sediments at Station 1 compared
626 to M92 (4100 μM during M136 and M137 versus 1800 μM during M92 within the first 8
627 cm of the core) (Fig. 4). Because of higher H_2S concentrations, Fe concentrations were
628 controlled by the solubility of Fe monosulfide minerals (FeS). It may seem
629 counterintuitive that the surface sediment was highly sulfidic, while the overlying water
630 column was oxygenated. In order to explain this observation, we need to consider the
631 role of mats of filamentous sulfur oxidizing bacteria in controlling H_2S concentrations
632 in surface sediments. (Gutiérrez et al., 2008; Noffke et al., 2012; Yücel et al., 2017).
633 During M92 these mats were generally abundant on the shelf and upper slope
634 (Sommer et al., 2016), thus limiting the extent of H_2S accumulation within surface
635 sediments. Previous studies demonstrated that mats of sulfur oxidizing bacteria can
636 disappear during periods of oxygenation (Gutiérrez et al., 2008). Consistent with this
637 previous finding, visual inspection of the seafloor using the video-guided MUC revealed
638 that the abundance of bacterial mats on the seafloor seemed greatly reduced, which
639 is most probably related to oxic bottom water conditions on the shallow shelf during
640 the coastal El Niño event. As these microaerophilic organisms tend to avoid high
641 oxygen concentrations they probably started to die off or withdraw into the sediment
642 once oxygen levels raised. We suggest that the disappearance of sulfide-oxidizing
643 bacteria under oxic conditions created a situation where H_2S accumulation in the
644 surface sediment and FeS precipitation limited the extent of Fe release into the bottom
645 water.

646

647 **4.2 Benthic cadmium cycling**

648 **4.2.1 Comparison of diffusive and in-situ benthic chamber cadmium fluxes**

649 At stations above and below the permanent OMZ (~~Stations~~Station 1, 9 and 10),
650 the slopes of Cd concentrations versus time during benthic chamber incubations were
651 largely consistent with theoretical Cd concentration gradients over time based on our
652 diffusive flux estimates (Fig. 7). In contrast, the fluxes determined with benthic
653 chambers at stations within the OMZ (Station 4, 5 and 6) were 25 to 40 times higher

654 than the diffusive flux (Table 3). This discrepancy demonstrates that diffusion cannot
655 be the dominant process leading to the continuous decrease of dissolved Cd during
656 benthic chamber incubations. Alternatively, Cd could be precipitated within the benthic
657 chamber and removed through downward sinking of Cd-rich particles. Cadmium
658 sulfide (greenockite) has a relatively low solubility compared to sulfide minerals of other
659 TMs ($\text{CdS} \ll \text{FeS}$). It is generally agreed that CdS precipitation can take place at trace
660 amounts of H_2S ($\text{H}_2\text{S} < 1 \mu\text{M}$, i.e., below the detection limit of the method applied in
661 this study) (Davies-Colley et al., 1985; Rosenthal et al., 1995). Previous studies using
662 in-situ benthic flux chambers have concluded that production of H_2S in the sediment
663 or the accumulation of H_2S in benthic chambers during incubations can switch the
664 direction of the Cd flux or intensify Cd removal through CdS precipitation (Westerlund
665 et al., 1986; Colbert et al., 2001). Precipitation of CdS during the incubation is,
666 therefore, a viable explanation for the discrepancy between diffusive Cd flux and Cd
667 fluxes in benthic chambers observed in our study. Furthermore, the three different
668 trends of Cd concentrations observed in benthic chamber incubations can be related
669 to H_2S concentrations in the surface sediment below the benthic chambers (Table 3).
670 At stations within the OMZ (~~Stations~~Station 4, 5 and 6), pore water H_2S concentrations
671 in surface sediments were moderate (few μM). It is likely that there was a continuous
672 leakage of trace amounts of H_2S from the pore water into the bottom waters during the
673 incubation, thus leading to CdS precipitation and declining Cd concentrations. On the
674 shallowest shelf station (Station 1), where pore water H_2S concentrations in the surface
675 sediment were high (hundreds of μM), a potentially large amount could have been
676 released at the beginning of the incubation, thus explaining pronounced Cd depletion
677 in the chamber compared to the surrounding bottom water (0.1 nM within the chamber
678 compared to 0.4 nM outside the chamber). Below the OMZ (~~Stations~~Station 9 and 10),
679 where there was no H_2S present in surface sediments, there was no Cd depletion in
680 the chamber during the incubation and, consistent with previous studies in oxic settings
681 (Westerlund et al., 1986; Ciceri et al., 1992; Zago et al., 2000; Turetta et al., 2005),
682 both diffusive and benthic chamber flux data were indicative of an upward-directed flux
683 out of the sediment. Due to the absence of H_2S , dissolved Cd released from biogenic
684 particles in the surface sediment could accumulate in the pore water thus driving a
685 diffusive flux out of the sediment.

686

687 **4.2.2 Quantification of the sedimentary cadmium sink**

688 Consistent with our Cd flux data there is general consent that OMZs are a sink
689 for Cd. Several water column studies have observed Cd depletion in water masses
690 within the Peruvian and other OMZs, which was mostly attributed to Cd removal via
691 CdS precipitation in sulfidic micro-niches within particles in the water column (Janssen
692 et al., 2014; Conway and John, 2015b). Sedimentary studies showed that Cd is highly
693 enriched in OMZ sediments, which has mostly been attributed to the delivery of Cd
694 with organic material and subsequent fixation as CdS within sulfidic sediments
695 (Ragueneau et al., 2000; Böning et al., 2004; Borchers et al., 2005; Muñoz et al., 2012;
696 Little et al., 2015). Based on our data, we can quantify the delivery of Cd to the
697 sediments via three different pathways: (1) diffusion across the sediment-water
698 interface and CdS precipitation within the sediment; (2) Cd incorporation by
699 phytoplankton and delivery to the sediment with organic matter; (3) CdS precipitation
700 in the water column and particulate delivery to the sediment (Table 3).

701 The enrichment of Cd in the sediment relative to the lithogenic background
702 (expressed as excess Cd concentration; Cd_{xs}) was calculated using the following
703 equation (Brumsack, 2006):

$$704 \quad Cd_{xs} = Cd_{sample} - Al_{sample} * (Cd/Al)_{crust} \quad (6)$$

705 The Cd/Al ratio of the upper continental crust ($1.22 \cdot 10^{-6}$) was used as lithogenic
706 background reference (Taylor and McLennan, 2009). To calculate the flux of Cd to the
707 sediment, Cd_{xs} was multiplied with the mass accumulation rate (MAR) from published
708 data for each individual site (Dale et al., 2015b). To approximate the amount of Cd
709 delivered to the sediment with organic material, the average concentration ratio of Cd
710 to C in phytoplankton (Moore et al., 2013) was multiplied by published particulate
711 organic carbon rain rates (maximum estimate) or burial rates (minimum estimate) for
712 each individual site (Dale et al., 2015b). The Cd delivery via precipitation in the water
713 column was determined as the remainder of $Cd_{xs} * MAR$ after subtraction of the two
714 other sources (i.e., diffusive flux and minimum/maximum delivery by organic material).

715 Sediments at all stations on the Peruvian shelf and slope are enriched in Cd
716 relative to the lithogenic background. The accumulation rate of Cd decreases with
717 distance from the coast from $250 \mu\text{mol m}^{-2} \text{y}^{-1}$ at Station 1 to $4 \mu\text{mol m}^{-2} \text{y}^{-1}$ at Station 9
718 (Table 3). These fluxes generally exceed the amount of Cd delivered to the sediments

719 via diffusion and associated with organic material. Together these mechanisms of Cd
720 delivery can only account for ~ 20 % of the Cd enrichment at stations above and inside
721 the permanent OMZ, with the delivery with organic material being of greater
722 importance. The remaining Cd enrichment in the sediment (~ 80 %), after subtraction
723 of diffusive and minimum/maximum organic Cd sources, must be related to CdS
724 precipitation in the water column and delivery of Cd-rich particles to the sediment. This
725 removal process can be a combination of CdS precipitation in sulfidic micro-niches
726 around sinking particles (Janssen et al., 2014; Bianchi et al., 2018), CdS precipitation
727 in sulfide plumes (Xie et al., 2019) when sedimentary H₂S can spread throughout the
728 water column (Schunck et al., 2013; Ohde, 2018), and precipitation of CdS in the near-
729 bottom water (this study). Our estimated CdS precipitation in the water column within
730 the OMZ agrees with the Cd fluxes determined from benthic chamber incubations,
731 where dissolved Cd removal takes place in the 20 – 30 cm of overlying water above
732 the seafloor. These Cd removal fluxes from benthic chambers alone are sufficient to
733 account for 41 % – 68 % of the estimated particulate Cd removal from the water column
734 and 38 % – 60 % of total Cd enrichment in the sediment within the OMZ (Table 3).
735 Considering that Cd precipitation in near-bottom water is unlikely to be restricted to the
736 20 – 30 cm above the seafloor, covered by our benthic chambers, the removal flux
737 associated with this process is likely to be even higher. At Station 1, where the surface
738 sediment below the benthic chamber was highly sulfidic, the particulate Cd removal
739 calculated from the concentration difference between the bottom water (0.5 m) and the
740 first sample from the benthic chamber incubation (taken after 0.25 h) was high enough
741 to explain the total Cd enrichment in the sediment.

742 Below the OMZ, at Station 9, where the smallest Cd enrichment was observed, the
743 relative contribution of Cd delivery with organic material increases. About half of the
744 Cd enrichment can be attributed to organic material at this station.

745 Once Cd is delivered to the sediment, it can either stay fixed in the solid phase
746 or be released to the pore waters. Cadmium concentrations in pore waters of
747 subsurface sediments (> 10 cm sediment depth) were mostly higher than bottom water
748 concentrations (Fig. 6), indicating a transfer of Cd from the solid phase into pore waters
749 during early diagenesis. Cadmium sulfides are considered highly insoluble and stable
750 within sediments (Elderfield et al., 1981), even upon re-oxygenation (Rosenthal et al.,
751 1995). Therefore, Cd release through re-dissolution of CdS is ruled out as a potential

752 source of dissolved Cd. Alternatively, Cd liberation upon remineralization of organic
753 material could explain elevated Cd concentrations in the pore water. Elevated Cd
754 concentrations in sulfidic pore waters have been observed in previous studies and
755 attributed to Cd stabilization through formation of organic and inorganic complexes
756 (Gobeil et al., 1987; Sundby et al., 2004). Experimental data gave evidence for the
757 presence of dissolved Cd bisulfide and polysulfide complexes in pore waters. An
758 increase of electrochemically active Cd after UV irradiation, was explained by the
759 destruction of electrochemically inactive bisulfide and polysulfide complexes (Gobeil et
760 al., 1987). At very high H₂S concentrations ($> 10^{-3}$ M) the solubility of Cd may increase
761 due to an increase in these bisulfide and polysulfide complexes. Under such highly
762 sulfidic conditions, Cd solubility may even exceed the solubility in oxygenated waters
763 and highly sulfidic sediment can eventually lead to a diffusive source of Cd to the
764 bottom water (Davies-Colley et al., 1985). Such a scenario may explain the negative
765 (i.e., upward-directed) diffusive Cd flux at Station 1, where the pore waters of surface
766 sediments are highly sulfidic.

767

768

769 **5. Conclusions and implications for trace metal sources and sinks in the future** 770 **ocean**

771 Consistent with earlier work, our results demonstrate that that OMZ sediments
772 are a source for Fe and a sink for Cd. Moreover, based on our findings, biogeochemical
773 conditions and processes that control the benthic fluxes of these ~~TM~~TMs across the
774 Peruvian OMZ can be further constrained.

775 Within the OMZ, where bottom dwelling macrofauna is absent, diffusion is the
776 main process that transports Fe from the sediment pore water into the bottom water.
777 The accumulation of high levels of H₂S in pore waters, modulated by the abundance
778 of sulfur oxidizing bacteria, can reduce diffusive Fe release through sulfide precipitation
779 within pore waters. In anoxic bottom waters Fe can be rapidly removed, likely via
780 oxidation with NO₂⁻ and/or interaction with particles. Benthic Cd fluxes are directed
781 from the bottom water into the sediment within the OMZ. Diffusive fluxes and delivery
782 of Cd via organic material cannot account for the sedimentary Cd enrichment. Instead

783 CdS precipitation in near-bottom waters could be the most important pathway that
784 delivers Cd to the sediments.

785 According to our results, H₂S concentrations in surface sediments exert a first
786 order control on the magnitude and direction of Fe and Cd fluxes across the sediment-
787 water interface. With generally decreasing oxygen concentrations in the ocean and an
788 expansion of OMZs (Stramma et al., 2008; Schmidtko et al., 2017), sulfidic surface
789 sediments will likely also expand. With regard to the solubility of their sulfide minerals,
790 Fe and Cd represent two opposite end members. The solubility of sulfide minerals of
791 other important nutrient-type TMs, such as Ni and Zn, is intermediate between those
792 of Fe and Cd (Fe > Ni > Zn > Cd). An expansion of sulfidic surface sediments is thus
793 likely to affect sedimentary TM fluxes in a differing manner. This notion is illustrated in
794 Fig. 10, showing saturation indices calculated based on the range of TM
795 concentrations observed in the ocean and typical H₂S concentrations observed in
796 anoxic marine environments (nM – μM concentrations represent sulfidic events in the
797 water column; μM – mM concentrations are typical for pore waters). Cadmium sulfide
798 minerals become oversaturated at nM to μM H₂S concentrations, which explains why
799 Cd removal can take place in the bottom water in OMZs. By contrast, FeS is highly
800 undersaturated under the typical biogeochemical conditions in the water column.
801 Therefore, FeS precipitation is unlikely to take place in the water column, even under
802 somewhat more reducing conditions. Other sulfide-forming TMs have an intermediate
803 sulfide solubility (e.g. Zn, Ni), which could imply that the direction and magnitude of
804 their sedimentary fluxes is susceptible to expanding ocean anoxia. The differing
805 response of TMs to an expansion of sulfidic conditions may cause a change in the TM
806 stoichiometry of upwelling water masses with potential consequences for TM-
807 dependent marine ecosystems in surface waters.

808

809

810 **Data availability**

811 The data will be made available at Pangaea upon publication of the article.

812

813

814 **Author contribution**

815 AP and FS conceived the study. AP, FS, AD, SS conducted the sampling at sea. AP
816 analyzed the trace metal concentrations. AP and FS prepared the manuscript with
817 contributions from all co-authors.

818

819

820 **Competing Interests**

821 The authors declare that they have no conflict of interest.

822

823

824 **Acknowledgements**

825 We are grateful for the support of the crew of RV Meteor during the fieldwork. For their
826 technical and analytical assistance we thank A. Beck, A. Bleyer, B. Domeyer, D.
827 Jasinski, A. Petersen, T. Steffens, R. Surberg and M. Türk. This study was supported
828 by the German Research Foundation through the Emmy Noether
829 Nachwuchsforschergruppe ICONOX (Iron Cycling in Continental Margin Sediments
830 and the Nutrient and Oxygen Balance of the Ocean) and Sonderforschungsbereich
831 754 (Climate-Biogeochemistry Interactions in the Tropical Ocean). We also would like
832 to thank Edouard Metzger and Michael Staubwasser for their constructive reviews, as
833 well as S. Wajih A. Naqvi for the editorial handling.

834 **References**

835

836 Audry, S., Blanc, G., Schäfer, J., Chaillou, G. and Robert, S.: Early diagenesis of
837 trace metals (Cd, Cu, Co, Ni, U, Mo, and V) in the freshwater reaches of a macrotidal
838 estuary, *Geochim. Cosmochim. Acta*, 70(9), 2264–2282,
839 doi:10.1016/j.gca.2006.02.001, 2006.

840 Ball, J. W. and Nordstrom, D. K.: WATEQ4F -- User's manual with revised
841 thermodynamic data base and test cases for calculating speciation of major, trace
842 and redox elements in natural waters, US Geol. Surv., (Open-File Rep.), 91–183,
843 doi:10.3133/ofr90129, 1991.

844 Bianchi, D., Weber, T. S., Kiko, R. and Deutsch, C.: Global niche of marine anaerobic
845 metabolisms expanded by particle microenvironments, *Nat. Geosci.*, 11(April), 1–6,
846 doi:10.1038/s41561-018-0081-0, 2018.

847 Biller, D. V. and Bruland, K. W.: Sources and distributions of Mn, Fe, Co, Ni, Cu, Zn,
848 and Cd relative to macronutrients along the central California coast during the spring
849 and summer upwelling season, *Mar. Chem.*, 155, 50–70,
850 doi:10.1016/j.marchem.2013.06.003, 2013.

851 Böning, P., Brumsack, H. J., Böttcher, M. E., Schnetger, B., Kriete, C., Kallmeyer, J.
852 and Borchers, S. L.: Geochemistry of Peruvian near-surface sediments, *Geochim.
853 Cosmochim. Acta*, 68(21), 4429–4451, doi:10.1016/j.gca.2004.04.027, 2004.

854 Bopp, L., Le Quéré, C., Heimann, M., Manning, A. C. and Monfray, P.: Climate-
855 induced oceanic oxygen fluxes: Implications for the contemporary carbon budget,
856 *Global Biogeochem. Cycles*, 16(2), 6-1-6–13, doi:10.1029/2001GB001445, 2002.

857 Borchers, S. L., Schnetger, B., Böning, P. and Brumsack, H.-J.: Geochemical
858 signatures of the Namibian diatom belt: Perennial upwelling and intermittent anoxia,
859 *Geochemistry, Geophys. Geosystems*, 6(6), doi:10.1029/2004GC000886, 2005.

860 Boudreau, B. P.: *Diagenetic Models and Their Implementation*, Springer., 1997.

861 Boyd, P. W. and Ellwood, M. J.: The biogeochemical cycle of iron in the ocean, *Nat.
862 Geosci.*, 3(10), 675–682, doi:10.1038/ngeo964, 2010.

863 Bruland, K. W. and Lohan, M. C.: Controls of Trace Metals in Seawater, in *Treatise*

864 on Geochemistry, pp. 23–47, Elsevier., 2003.

865 Brumsack, H. J.: The trace metal content of recent organic carbon-rich sediments:
866 Implications for Cretaceous black shale formation, *Palaeogeogr. Palaeoclimatol.*
867 *Palaeoecol.*, 232(2–4), 344–361, doi:10.1016/j.palaeo.2005.05.011, 2006.

868 Canfield, D. E.: Reactive iron in marine sediments, *Geochim. Cosmochim. Acta*,
869 53(3), 619–632, doi:10.1016/0016-7037(89)90005-7, 1989.

870 Carlson, H. K., Clark, I. C., Blazewicz, S. J., Iavarone, A. T. and Coates, J. D.: Fe(II)
871 Oxidation Is an Innate Capability of Nitrate-Reducing Bacteria That Involves Abiotic
872 and Biotic Reactions, *J. Bacteriol.*, 195(14), 3260–3268, doi:10.1128/JB.00058-13,
873 2013.

874 Ciceri, G., Maran, C., Martinotti, W. and Queirazza, G.: Geochemical cycling of heavy
875 metals in a marine coastal area: benthic flux determination from pore water profiles
876 and in situ measurements using benthic chambers, *Hydrobiologia*, 235–236(1), 501–
877 517, doi:10.1007/BF00026238, 1992.

878 Colbert, D., Coale, K. ., Berelson, W. . and Johnson, K. .: Cadmium Flux in Los
879 Angeles/Long Beach Harbours and at Sites along the California Continental Margin,
880 *Estuar. Coast. Shelf Sci.*, 53(2), 169–180, doi:10.1006/ecss.2001.0802, 2001.

881 Collier, R. and Edmond, J.: The trace element geochemistry of marine biogenic
882 particulate matter, *Prog. Oceanogr.*, 13(2), 113–199, doi:10.1016/0079-
883 6611(84)90008-9, 1984.

884 Conway, T. M. and John, S. G.: Quantification of dissolved iron sources to the North
885 Atlantic Ocean, *Nature*, 511(7508), 212–215, doi:10.1038/nature13482, 2014.

886 Conway, T. M. and John, S. G.: Biogeochemical cycling of cadmium isotopes along a
887 high-resolution section through the North Atlantic Ocean, *Geochim. Cosmochim.*
888 *Acta*, 148, 269–283, doi:10.1016/j.gca.2014.09.032, 2015a.

889 Conway, T. M. and John, S. G.: The cycling of iron, zinc and cadmium in the North
890 East Pacific Ocean - Insights from stable isotopes, *Geochim. Cosmochim. Acta*, 164,
891 262–283, doi:10.1016/j.gca.2015.05.023, 2015b.

892 Dale, A. W., Nickelsen, L., Scholz, F., Hensen, C., Oeschlies, A. and Wallmann, K.: A
893 revised global estimate of dissolved iron fluxes from marine sediments, *Global*

894 Biogeochem. Cycles, 29(5), 691–707, doi:10.1002/2014GB005017, 2015a.

895 Dale, A. W., Sommer, S., Lomnitz, U., Montes, I., Treude, T., Liebetrau, V., Gier, J.,
896 Hensen, C., Dengler, M., Stolpovsky, K., Bryant, L. D. and Wallmann, K.: Organic
897 carbon production, mineralisation and preservation on the Peruvian margin,
898 Biogeosciences, 12(5), 1537–1559, doi:10.5194/bg-12-1537-2015, 2015b.

899 Dalsgaard, T., Thamdrup, B., Farías, L. and Revsbech, N. P.: Anammox and
900 denitrification in the oxygen minimum zone of the eastern South Pacific, Limnol.
901 Oceanogr., 57(5), 1331–1346, doi:10.4319/lo.2012.57.5.1331, 2012.

902 Davies-Colley, R. J., Nelson, P. O. and Williamson, K. J.: Sulfide control of cadmium
903 and copper concentrations in anaerobic estuarine sediments, Mar. Chem., 16(2),
904 173–186, doi:10.1016/0304-4203(85)90021-0, 1985.

905 Echevin, V., Colas, F., Espinoza-Morriberon, D., Vasquez, L., Anculle, T. and
906 Gutierrez, D.: Forcings and Evolution of the 2017 Coastal El Niño Off Northern Peru
907 and Ecuador, Front. Mar. Sci., 5(October), 1–16, doi:10.3389/fmars.2018.00367,
908 2018.

909 Ehlert, C., Doering, K., Wallmann, K., Scholz, F., Sommer, S., Grasse, P., Geilert, S.
910 and Frank, M.: Stable silicon isotope signatures of marine pore waters – Biogenic
911 opal dissolution versus authigenic clay mineral formation, Geochim. Cosmochim.
912 Acta, 191, 102–117, doi:10.1016/j.gca.2016.07.022, 2016.

913 Elderfield, H., McCaffrey, R. J., Luedtke, N., Bender, M. and Truesdale, V. W.:
914 Chemical diagenesis in Narragansett Bay sediments, Am. J. Sci., 281(8), 1021–1055,
915 doi:10.2475/ajs.281.8.1021, 1981.

916 Elrod, V. A., Berelson, W. M., Coale, K. H. and Johnson, K. S.: The flux of iron from
917 continental shelf sediments: A missing source for global budgets, Geophys. Res.
918 Lett., 31(12), n/a-n/a, doi:10.1029/2004GL020216, 2004.

919 Fitzsimmons, J. N., Conway, T. M., Lee, J.-M., Kayser, R., Thyng, K. M., John, S. G.
920 and Boyle, E. A.: Dissolved iron and iron isotopes in the southeastern Pacific Ocean,
921 Global Biogeochem. Cycles, 30(10), 1372–1395, doi:10.1002/2015GB005357, 2016.

922 Friedrich, J., Dinkel, C., Friedl, G., Pimenov, N., Wijsman, J., Gomoiu, M.-T.,
923 Cociasu, A., Popa, L. and Wehrli, B.: Benthic Nutrient Cycling and Diagenetic
924 Pathways in the North-western Black Sea, Estuar. Coast. Shelf Sci., 54(3), 369–383,

925 doi:10.1006/ecss.2000.0653, 2002.

926 Garreaud, R. D.: A plausible atmospheric trigger for the 2017 coastal El Niño, *Int. J.*
927 *Climatol.*, 38(January 2017), e1296–e1302, doi:10.1002/joc.5426, 2018.

928 Gendron, A., Silverberg, N., Sundby, B. and Lebel, J.: Early diagenesis of cadmium
929 and cobalt in sediments of the Laurentian Trough, *Geochim. Cosmochim. Acta*,
930 50(5), 741–747, doi:10.1016/j.ijmachtools.2007.10.013, 1986.

931 Gerringa, L. J. A.: Aerobic degradation of organic matter and the mobility of Cu, Cd,
932 Ni, Pb, Zn, Fe and Mn in marine sediment slurries, *Mar. Chem.*, 29(C), 355–374,
933 doi:10.1016/0304-4203(90)90023-6, 1990.

934 Gobeil, C., Silverberg, N., Sundby, B. and Cossa, D.: Cadmium diagenesis in
935 Laurentian Trough sediments, *Geochim. Cosmochim. Acta*, 51(3), 589–596,
936 doi:10.1016/0016-7037(87)90071-8, 1987.

937 Graco, M. I., Purca, S., Dewitte, B., Castro, C. G., Morón, O., Ledesma, J., Flores, G.
938 and Gutiérrez, D.: The OMZ and nutrient features as a signature of interannual and
939 low-frequency variability in the Peruvian upwelling system, *Biogeosciences*, 14(20),
940 4601–4617, doi:10.5194/bg-14-4601-2017, 2017.

941 Grasshoff, M., Erhardt, M. and Kremling, K.: *Methods of seawater analysis.*, Wiley-
942 VCH, Weinheim, doi:10.1002/ange.19770890738, 1999.

943 Gutiérrez, D., Enríquez, E., Purca, S., Quipúzcoa, L., Marquina, R., Flores, G. and
944 Graco, M.: Oxygenation episodes on the continental shelf of central Peru: Remote
945 forcing and benthic ecosystem response, *Prog. Oceanogr.*, 79(2–4), 177–189,
946 doi:10.1016/j.pocean.2008.10.025, 2008.

947 Hawco, N. J., Ohnemus, D. C., Resing, J. A., Twining, B. S. and Saito, M. A.: A
948 dissolved cobalt plume in the oxygen minimum zone of the eastern tropical South
949 Pacific, *Biogeosciences*, 13(20), 5697–5717, doi:10.5194/bg-13-5697-2016, 2016.

950 Heller, M. I., Lam, P. J., Moffett, J. W., Till, C. P., Lee, J. M., Toner, B. M. and
951 Marcus, M. A.: Accumulation of Fe oxyhydroxides in the Peruvian oxygen deficient
952 zone implies non-oxygen dependent Fe oxidation, *Geochim. Cosmochim. Acta*, 211,
953 174–193, doi:10.1016/j.gca.2017.05.019, 2017.

954 Helm, K. P., Bindoff, N. L. and Church, J. A.: Observed decreases in oxygen content

955 of the global ocean, *Geophys. Res. Lett.*, 38(23), 1–6, doi:10.1029/2011GL049513,
956 2011.

957 Homoky, W. B., Severmann, S., McManus, J., Berelson, W. M., Riedel, T. E.,
958 Statham, P. J. and Mills, R. A.: Dissolved oxygen and suspended particles regulate
959 the benthic flux of iron from continental margins, *Mar. Chem.*, 134–135, 59–70,
960 doi:10.1016/j.marchem.2012.03.003, 2012.

961 Hydes, D., Aoyama, M., Aminot, A., Bakker, K., Becker, S., Coverly, S., Daniel, A.,
962 Dickson, A. G., Grosso, O., Kerouel, R., van Ooijen, J., Sato, K., Tanhua, T.,
963 Woodward, E. M. S. and Zhang, J. Z.: Determination of dissolved nutrients (N, P, Si)
964 in seawater with high precision and inter-comparability using gas-segmented
965 continuous flow analysers, *Go-sh. Repeat Hydrogr. Man. IOCCP Rep. A Collect.*
966 *Expert Reports Guidel.*, 134(14), 1–87 [online] Available from:
967 <http://archimer.ifremer.fr/doc/00020/13141/>, 2010.

968 Janssen, D. J., Conway, T. M., John, S. G., Christian, J. R., Kramer, D. I., Pedersen,
969 T. F. and Cullen, J. T.: Undocumented water column sink for cadmium in open ocean
970 oxygen-deficient zones, *Proc. Natl. Acad. Sci.*, 111(19), 6888–6893,
971 doi:10.1073/pnas.1402388111, 2014.

972 John, S. G., Helgoe, J., Townsend, E., Weber, T., DeVries, T., Tagliabue, A., Moore,
973 K., Lam, P., Marsay, C. M. and Till, C.: Biogeochemical cycling of Fe and Fe stable
974 isotopes in the Eastern Tropical South Pacific, *Mar. Chem.*, 201(March), 66–76,
975 doi:10.1016/j.marchem.2017.06.003, 2018.

976 Karstensen, J., Stramma, L. and Visbeck, M.: Oxygen minimum zones in the eastern
977 tropical Atlantic and Pacific oceans, *Prog. Oceanogr.*, 77(4), 331–350,
978 doi:10.1016/j.pocean.2007.05.009, 2008.

979 Keeling, R. F., Körtzinger, A. and Gruber, N.: Ocean Deoxygenation in a Warming
980 World, *Ann. Rev. Mar. Sci.*, 2(1), 199–229,
981 doi:10.1146/annurev.marine.010908.163855, 2010.

982 Klar, J. K., Schlosser, C., Milton, J. A., Woodward, E. M. S., Lacan, F., Parkinson, I.
983 J., Achterberg, E. P. and James, R. H.: Sources of dissolved iron to oxygen minimum
984 zone waters on the Senegalese continental margin in the tropical North Atlantic
985 Ocean: Insights from iron isotopes, *Geochim. Cosmochim. Acta*, 236, 60–78,

986 doi:10.1016/j.gca.2018.02.031, 2018.

987 Klinkhammer, G., Heggie, D. T. and Graham, D. W.: Metal diagenesis in oxic marine
988 sediments, *Earth Planet. Sci. Lett.*, 61(2), 211–219, doi:10.1016/0012-
989 821X(82)90054-1, 1982.

990 Klueglein, N. and Kappler, A.: Abiotic oxidation of Fe(II) by reactive nitrogen species
991 in cultures of the nitrate-reducing Fe(II) oxidizer *Acidovorax* sp. BoFeN1 - questioning
992 the existence of enzymatic Fe(II) oxidation, *Geobiology*, 11(2), 180–190,
993 doi:10.1111/gbi.12019, 2013.

994 Lam, P. and Kuypers, M. M. M.: Microbial Nitrogen Cycling Processes in Oxygen
995 Minimum Zones, *Ann. Rev. Mar. Sci.*, 3(1), 317–345, doi:10.1146/annurev-marine-
996 120709-142814, 2011.

997 Lam, P., Lavik, G., Jensen, M. M., van de Vossenberg, J., Schmid, M., Woebken, D.,
998 Gutierrez, D., Amann, R., Jetten, M. S. M. and Kuypers, M. M. M.: Revising the
999 nitrogen cycle in the Peruvian oxygen minimum zone, *Proc. Natl. Acad. Sci.*, 106(12),
1000 4752–4757, doi:10.1073/pnas.0812444106, 2009.

1001 Lane, T. W. and Morel, F. M. M.: A biological function for cadmium in marine diatoms,
1002 *Proc. Natl. Acad. Sci.*, 97(9), 4627–4631, doi:10.1073/pnas.090091397, 2000.

1003 Lee, J. and Morel, F.: Replacement of zinc by cadmium in marine phytoplankton,
1004 *Mar. Ecol. Prog. Ser.*, 127(1–3), 305–309, doi:10.3354/meps127305, 1995.

1005 Lenstra, W. K., Hermans, M., Séguret, M. J. M., Witbaard, R., Behrends, T., Dijkstra,
1006 N., van Helmond, N. A. G. M., Kraal, P., Laan, P., Rijkenberg, M. J. A., Severmann,
1007 S., Teacă, A. and Slomp, C. P.: The shelf-to-basin iron shuttle in the Black Sea
1008 revisited, *Chem. Geol.*, 511(April), 314–341, doi:10.1016/j.chemgeo.2018.10.024,
1009 2019.

1010 Levin, L., Gutiérrez, D., Rathburn, A., Neira, C., Sellanes, J., Muñoz, P., Gallardo, V.
1011 and Salamanca, M.: Benthic processes on the Peru margin: a transect across the
1012 oxygen minimum zone during the 1997–98 El Niño, *Prog. Oceanogr.*, 53(1), 1–27,
1013 doi:10.1016/S0079-6611(02)00022-8, 2002.

1014 Li, Y.-H. and Gregory, S.: Diffusion of ions in sea water and in deep-sea sediments,
1015 *Geochim. Cosmochim. Acta*, 38(5), 703–714, doi:10.1016/0016-7037(74)90145-8,
1016 1974.

1017 Little, S. H., Vance, D., Lyons, T. W. and McManus, J.: Controls on trace metal
1018 authigenic enrichment in reducing sediments: Insights from modern oxygen-deficient
1019 settings, *Am. J. Sci.*, 315(2), 77–119, doi:10.2475/02.2015.01, 2015.

1020 Liu, X. and Millero, F. J.: The solubility of iron in seawater, *Mar. Chem.*, 77(1), 43–54,
1021 doi:10.1016/S0304-4203(01)00074-3, 2002.

1022 Lohan, M. C. and Bruland, K. W.: Elevated Fe(II) and dissolved Fe in hypoxic shelf
1023 waters off Oregon and Washington: An enhanced source of iron to coastal upwelling
1024 regimes, *Environ. Sci. Technol.*, 42(17), 6462–6468, doi:10.1021/es800144j, 2008.

1025 Metzger, E., Simonucci, C., Viollier, E., Sarazin, G., Prévot, F., Elbaz-Poulichet, F.,
1026 Seidel, J.-L. and Jézéquel, D.: Influence of diagenetic processes in Thau lagoon on
1027 cadmium behavior and benthic fluxes, *Estuar. Coast. Shelf Sci.*, 72(3), 497–510,
1028 doi:10.1016/j.ecss.2006.11.016, 2007.

1029 Moore, C. M., Mills, M. M., Arrigo, K. R., Berman-Frank, I., Bopp, L., Boyd, P. W.,
1030 Galbraith, E. D., Geider, R. J., Guieu, C., Jaccard, S. L., Jickells, T. D., La Roche, J.,
1031 Lenton, T. M., Mahowald, N. M., Marañón, E., Marinov, I., Moore, J. K., Nakatsuka,
1032 T., Oschlies, A., Saito, M. A., Thingstad, T. F., Tsuda, A. and Ulloa, O.: Processes
1033 and patterns of oceanic nutrient limitation, *Nat. Geosci.*, 6(9), 701–710,
1034 doi:10.1038/ngeo1765, 2013.

1035 Morel, F. M. M., Milligan, A. J. and Saito, M. A.: Marine Bioinorganic Chemistry: The
1036 Role of Trace Metals in the Oceanic Cycles of Major Nutrients, in *Treatise on*
1037 *Geochemistry*, vol. 197, pp. 123–150, Elsevier., 2014.

1038 Morse, J. W. and Luther, G. W.: Chemical influences on trace metal-sulfide
1039 interactions in anoxic sediments, *Geochim. Cosmochim. Acta*, 63(19–20), 3373–
1040 3378, doi:10.1016/S0016-7037(99)00258-6, 1999.

1041 Muñoz, P., Dezileau, L., Cardenas, L., Sellanes, J., Lange, C. B., Inostroza, J.,
1042 Muratli, J. and Salamanca, M. A.: Geochemistry of trace metals in shelf sediments
1043 affected by seasonal and permanent low oxygen conditions off central Chile, SE
1044 Pacific (~36°S), *Cont. Shelf Res.*, 33, 51–68, doi:10.1016/j.csr.2011.11.006, 2012.

1045 Noble, A. E., Lamborg, C. H., Ohnemus, D. C., Lam, P. J., Goepfert, T. J., Measures,
1046 C. I., Frame, C. H., Casciotti, K. L., DiTullio, G. R., Jennings, J. and Saito, M. A.:
1047 Basin-scale inputs of cobalt, iron, and manganese from the Benguela-Angola front to

1048 the South Atlantic Ocean, *Limnol. Oceanogr.*, 57(4), 989–1010,
1049 doi:10.4319/lo.2012.57.4.0989, 2012.

1050 Noffke, A., Hensen, C., Sommer, S., Scholz, F., Bohlen, L., Mosch, T., Graco, M. and
1051 Wallmann, K.: Benthic iron and phosphorus fluxes across the Peruvian oxygen
1052 minimum zone, *Limnol. Oceanogr.*, 57(3), 851–867, doi:10.4319/lo.2012.57.3.0851,
1053 2012.

1054 Ohde, T.: Coastal Sulfur Plumes off Peru During El Niño, La Niña, and Neutral
1055 Phases, *Geophys. Res. Lett.*, 45(14), 7075–7083, doi:10.1029/2018GL077618, 2018.

1056 Olson, L., Quinn, K. A., Siebecker, M. G., Luther, G. W., Hastings, D. and Morford, J.
1057 L.: Trace metal diagenesis in sulfidic sediments: Insights from Chesapeake Bay,
1058 *Chem. Geol.*, 452, 47–59, doi:10.1016/j.chemgeo.2017.01.018, 2017.

1059 Oschlies, A., Schulz, K. G., Riebesell, U. and Schmittner, A.: Simulated 21st
1060 century's increase in oceanic suboxia by CO₂-enhanced biotic carbon export, *Global*
1061 *Biogeochem. Cycles*, 22(4), 1–10, doi:10.1029/2007GB003147, 2008.

1062 [Pakhomova, S. V., Hall, P. O. J., Kononets, M. Y., Rozanov, A. G., Tengberg, A. and](#)
1063 [Vershinin, A. V.: Fluxes of iron and manganese across the sediment–water interface](#)
1064 [under various redox conditions, *Mar. Chem.*, 107\(3\), 319–331,](#)
1065 [doi:10.1016/j.marchem.2007.06.001, 2007.](#)

1066 Peng, Q., Xie, S.-P., Wang, D., Zheng, X.-T. and Zhang, H.: Coupled ocean-
1067 atmosphere dynamics of the 2017 extreme coastal El Niño, *Nat. Commun.*, 10(1),
1068 298, doi:10.1038/s41467-018-08258-8, 2019.

1069 Pennington, J. T., Mahoney, K. L., Kuwahara, V. S., Kolber, D. D., Calienes, R. and
1070 Chavez, F. P.: Primary production in the eastern tropical Pacific: A review, *Prog.*
1071 *Oceanogr.*, 69(2–4), 285–317, doi:10.1016/j.pocean.2006.03.012, 2006.

1072 Point, D., Monperrus, M., Tessier, E., Amouroux, D., Chauvaud, L., Thouzeau, G.,
1073 Jean, F., Amice, E., Grall, J., Leynaert, A., Clavier, J. and Donard, O. F. X.: Biological
1074 control of trace metal and organometal benthic fluxes in a eutrophic lagoon (Thau
1075 Lagoon, Mediterranean Sea, France), *Estuar. Coast. Shelf Sci.*, 72(3), 457–471,
1076 doi:10.1016/j.ecss.2006.11.013, 2007.

1077 Price, N. M. and Morel, F. M. M.: Cadmium and cobalt substitution for zinc in a
1078 marine diatom, *Nature*, 344(6267), 658–660, doi:10.1038/344658a0, 1990.

1079 Ragueneau, O., Tréguer, P., Leynaert, A., Anderson, R. F., Brzezinski, M. A.,
1080 DeMaster, D. J., Dugdale, R. C., Dymond, J., Fischer, G., François, R., Heinze, C.,
1081 Maier-Reimer, E., Martin-Jézéquel, V., Nelson, D. M. and Quéguiner, B.: A review of
1082 the Si cycle in the modern ocean: Recent progress and missing gaps in the
1083 application of biogenic opal as a paleoproductivity proxy, *Glob. Planet. Change*,
1084 26(4), 317–365, doi:10.1016/S0921-8181(00)00052-7, 2000.

1085 Raiswell, R. and Canfield, D. E.: The Iron Biogeochemical Cycle Past and Present,
1086 *Geochemical Perspect.*, 1(1), 1–220, doi:10.7185/geochempers.1.1, 2012.

1087 Rapp, I., Schlosser, C., Rusiecka, D., Gledhill, M. and Achterberg, E. P.: Automated
1088 preconcentration of Fe, Zn, Cu, Ni, Cd, Pb, Co, and Mn in seawater with analysis
1089 using high-resolution sector field inductively-coupled plasma mass spectrometry,
1090 *Anal. Chim. Acta*, 976, 1–13, doi:10.1016/j.aca.2017.05.008, 2017.

1091 Rapp, I., Schlosser, C., Menzel Barraqueta, J.-L., Wenzel, B., Lüdke, J., Scholten, J.,
1092 Gasser, B., Reichert, P., Gledhill, M., Dengler, M. and Achterberg, E. P.: Controls on
1093 redox-sensitive trace metals in the Mauritanian oxygen minimum zone,
1094 *Biogeosciences Discuss.*, (November), 1–49, doi:10.5194/bg-2018-472, 2018.

1095 Rickard, D., Griffith, A., Oldroyd, A., Butler, I. B., Lopez-Capel, E., Manning, D. A. C.
1096 and Apperley, D. C.: The composition of nanoparticulate mackinawite, tetragonal
1097 iron(II) monosulfide, *Chem. Geol.*, 235(3–4), 286–298,
1098 doi:10.1016/j.chemgeo.2006.07.004, 2006.

1099 Rigaud, S., Radakovitch, O., Couture, R. M., Deflandre, B., Cossa, D., Garnier, C.
1100 and Garnier, J. M.: Mobility and fluxes of trace elements and nutrients at the
1101 sediment-water interface of a lagoon under contrasting water column oxygenation
1102 conditions, *Appl. Geochemistry*, 31(April 2013), 35–51,
1103 doi:10.1016/j.apgeochem.2012.12.003, 2013.

1104 Rosenthal, Y., Lam, P., Boyle, E. A. and Thomson, J.: Precipitation and
1105 postdepositional mobility, *Earth Planet. Sci. Lett.*, 132, 99–111, doi:10.1016/0012-
1106 821X(95)00056-I, 1995.

1107 Rue, E. L. and Bruland, K. W.: The role of organic complexation on ambient iron
1108 chemistry in the equatorial Pacific Ocean and the response of a mesoscale iron
1109 addition experiment, *Limnol. Oceanogr.*, 42(5), 901–910,

1110 doi:10.4319/lo.1997.42.5.0901, 1997.

1111 Saito, M. A., Goepfert, T. J. and Ritt, J. T.: Some thoughts on the concept of
1112 colimitation: Three definitions and the importance of bioavailability, *Limnol.*
1113 *Oceanogr.*, 53(1), 276–290, doi:10.4319/lo.2008.53.1.0276, 2008.

1114 Schlosser, C., Streu, P., Frank, M., Lavik, G., Croot, P. L., Dengler, M. and
1115 Achterberg, E. P.: H₂S events in the Peruvian oxygen minimum zone facilitate
1116 enhanced dissolved Fe concentrations, *Sci. Rep.*, 8(1), 1–8, doi:10.1038/s41598-
1117 018-30580-w, 2018.

1118 Schmidtko, S., Stramma, L. and Visbeck, M.: Decline in global oceanic oxygen
1119 content during the past five decades, *Nature*, 542(7641), 335–339,
1120 doi:10.1038/nature21399, 2017.

1121 Scholz, F. and Neumann, T.: Trace element diagenesis in pyrite-rich sediments of the
1122 Achterwasser lagoon, SW Baltic Sea, *Mar. Chem.*, 107(4), 516–532,
1123 doi:10.1016/j.marchem.2007.08.005, 2007.

1124 Scholz, F., Mcmanus, J., Mix, A. C., Hensen, C. and Schneider, R. R.: The impact of
1125 ocean deoxygenation on iron release from continental margin sediments, *Nat.*
1126 *Geosci.*, 7(6), 433–437, doi:10.1038/ngeo2162, 2014.

1127 Scholz, F., Löscher, C. R., Fiskal, A., Sommer, S., Hensen, C., Lomnitz, U., Wuttig,
1128 K., Göttlicher, J., Kossel, E., Steininger, R. and Canfield, D. E.: Nitrate-dependent
1129 iron oxidation limits iron transport in anoxic ocean regions, *Earth Planet. Sci. Lett.*,
1130 454, 272–281, doi:10.1016/j.epsl.2016.09.025, 2016.

1131 Scholz, F., Schmidt, M., Hensen, C., Eroglu, S., Geilert, S., Gutjahr, M. and
1132 Liebetrau, V.: Shelf-to-basin iron shuttle in the Guaymas Basin, Gulf of California,
1133 *Geochim. Cosmochim. Acta*, 261, 76–92, doi:10.1016/j.gca.2019.07.006, 2019.

1134 Schunck, H., Lavik, G., Desai, D. K., Großkopf, T., Kalvelage, T., Löscher, C. R.,
1135 Paulmier, A., Contreras, S., Siegel, H., Holtappels, M., Rosenstiel, P., Schilhabel, M.
1136 B., Graco, M., Schmitz, R. A., Kuypers, M. M. M. and LaRoche, J.: Giant Hydrogen
1137 Sulfide Plume in the Oxygen Minimum Zone off Peru Supports
1138 Chemolithoautotrophy, *PLoS One*, 8(8), doi:10.1371/journal.pone.0068661, 2013.

1139 Scor Working Group: GEOTRACES – An international study of the global marine
1140 biogeochemical cycles of trace elements and their isotopes, *Geochemistry*, 67(2),

1141 85–131, doi:10.1016/j.chemer.2007.02.001, 2007.

1142 Severmann, S., McManus, J., Berelson, W. M. and Hammond, D. E.: The continental
1143 shelf benthic iron flux and its isotope composition, *Geochim. Cosmochim. Acta*,
1144 74(14), 3984–4004, doi:10.1016/j.gca.2010.04.022, 2010.

1145 Sommer, S., Linke, P., Pfannkuche, O., Schleicher, T., Schneider v. D, D., Reitz, A.,
1146 Haeckel, M., Flögel, S. and Hensen, C.: Seabed methane emissions and the habitat
1147 of frenulate tubeworms on the Captain Arutyunov mud volcano (Gulf of Cadiz), *Mar.*
1148 *Ecol. Prog. Ser.*, 382, 69–86, doi:10.3354/meps07956, 2009.

1149 Sommer, S., Gier, J., Treude, T., Lomnitz, U., Dengler, M., Cardich, J. and Dale, A.
1150 W.: Depletion of oxygen, nitrate and nitrite in the Peruvian oxygen minimum zone
1151 cause an imbalance of benthic nitrogen fluxes, *Deep. Res. Part I Oceanogr. Res.*
1152 *Pap.*, 112(3), 113–122, doi:10.1016/j.dsr.2016.03.001, 2016.

1153 Stookey, L. L.: Ferrozine---a new spectrophotometric reagent for iron, *Anal. Chem.*,
1154 42(7), 779–781, doi:10.1021/ac60289a016, 1970.

1155 Stramma, L., Johnson, G. C., Sprintall, J. and Mohrholz, V.: Expanding Oxygen-
1156 Minimum Zones in the Tropical Oceans, *Science (80-.)*, 320(5876), 655–658,
1157 doi:10.1126/science.1153847, 2008.

1158 Stramma, L., Schmidtko, S., Levin, L. A. and Johnson, G. C.: Ocean oxygen minima
1159 expansions and their biological impacts, *Deep. Res. Part I Oceanogr. Res. Pap.*,
1160 57(4), 587–595, doi:10.1016/j.dsr.2010.01.005, 2010.

1161 Straub, K. L., Benz, M., Schink, B. and Widdel, F.: Anaerobic, nitrate-dependent
1162 microbial oxidation of ferrous iron. *Appl Environ Microbiol*, *Appl. Environ. Microbiol.*,
1163 62(4), 1458–60, 1996.

1164 Sunda, W. G. and Huntsman, S. A.: Effect of Zn, Mn, and Fe on Cd accumulation in
1165 phytoplankton: Implications for oceanic Cd cycling, *Limnol. Oceanogr.*, 45(7), 1501–
1166 1516, doi:10.4319/lo.2000.45.7.1501, 2000.

1167 Sundby, B., Martinez, P. and Gobeil, C.: Comparative geochemistry of cadmium,
1168 rhenium, uranium, and molybdenum in continental margin sediments, *Geochim.*
1169 *Cosmochim. Acta*, 68(11), 2485–2493, doi:10.1016/j.gca.2003.08.011, 2004.

1170 Taylor, S. R. and McLennan, S. M.: Planetary crusts: Their composition, origin and

1171 evolution , by Stuart Ross Taylor and Scott M. McLennan, *Meteorit. Planet. Sci.*,
1172 44(3), 465–466, doi:10.1111/j.1945-5100.2009.tb00744.x, 2009.

1173 Thamdrup, B., Dalsgaard, T. and Revsbech, N. P.: Widespread functional anoxia in
1174 the oxygen minimum zone of the Eastern South Pacific, *Deep Sea Res. Part I*
1175 *Oceanogr. Res. Pap.*, 65, 36–45, doi:10.1016/j.dsr.2012.03.001, 2012.

1176 Turetta, C., Capodaglio, G., Cairns, W., Rabar, S. and Cescon, P.: Benthic fluxes of
1177 trace metals in the lagoon of Venice, *Microchem. J.*, 79(1–2), 149–158,
1178 doi:10.1016/j.microc.2004.06.003, 2005.

1179 Twining, B. S. and Baines, S. B.: The Trace Metal Composition of Marine
1180 Phytoplankton, *Ann. Rev. Mar. Sci.*, 5(1), 191–215, doi:10.1146/annurev-marine-
1181 121211-172322, 2013.

1182 Vedamati, J., Goepfert, T. and Moffett, J. W.: Iron speciation in the eastern tropical
1183 south pacific oxygen minimum zone off peru, *Limnol. Oceanogr.*, 59(6), 1945–1957,
1184 doi:10.4319/lo.2014.59.6.1945, 2014.

1185 Westerlund, S. F. G., Anderson, L. G., Hall, P. O. J., Iverfeldt, Å., Van Der Loeff, M.
1186 M. R. and Sundby, B.: Benthic fluxes of cadmium, copper, nickel, zinc and lead in the
1187 coastal environment, *Geochim. Cosmochim. Acta*, 50(6), 1289–1296,
1188 doi:10.1016/0016-7037(86)90412-6, 1986.

1189 Xie, R. C., Rehkämper, M., Grasse, P., van de Flierdt, T., Frank, M. and Xue, Z.:
1190 Isotopic evidence for complex biogeochemical cycling of Cd in the eastern tropical
1191 South Pacific, *Earth Planet. Sci. Lett.*, 512, 134–146, doi:10.1016/j.epsl.2019.02.001,
1192 2019.

1193 Xu, Y., Feng, L., Jeffrey, P. D., Shi, Y. and Morel, F. M. M.: Structure and metal
1194 exchange in the cadmium carbonic anhydrase of marine diatoms, *Nature*, 452(7183),
1195 56–61, doi:10.1038/nature06636, 2008.

1196 Yücel, M., Sommer, S., Dale, A. W. and Pfannkuche, O.: Microbial sulfide filter along
1197 a benthic redox gradient in the Eastern Gotland Basin, Baltic Sea, *Front. Microbiol.*,
1198 8(FEB), 1–16, doi:10.3389/fmicb.2017.00169, 2017.

1199 Zago, C., Capodaglio, G., Ceradini, S., Ciceri, G., Abelmoschi, L., Soggia, F.,
1200 Cescon, P. and Scarponi, G.: Benthic fluxes of cadmium, lead, copper and nitrogen
1201 species in the northern Adriatic Sea in front of the River Po outflow, Italy, *Sci. Total*

1202 Environ., 246(2–3), 121–137, doi:10.1016/S0048-9697(99)00421-0, 2000.

1203 Zumft, W. G.: Cell biology and molecular basis of denitrification., Microbiol. Mol. Biol.

1204 Rev., 61(4), 533–616 [online] Available from:

1205 <http://www.ncbi.nlm.nih.gov/pubmed/9409151>[http://www.pubmedcentral.nih.gov/](http://www.pubmedcentral.nih.gov/articlerender.fcgi?artid=PMC232623)

1206 [articlerender.fcgi?artid=PMC232623](http://www.pubmedcentral.nih.gov/articlerender.fcgi?artid=PMC232623), 1997.

1207

1208 **Figure captions**

1209

1210 Fig. 1: Sampling stations on the Peruvian continental margin during cruises M136 &
1211 M137 along a latitudinal depth transect at 12° S. The sampling stations for pore
1212 waters are depicted by white stars, for bottom waters by yellow dots and for benthic
1213 chamber incubations by red dots.

1214 Fig. 2: Oxygen, nitrate, nitrite and hydrogen sulfide concentrations on the Peruvian
1215 slope (Station 10, 1000 m depth), crossing the oxygen minimum zone (upper panel),
1216 and the upper shelf (Station 1, 75 m depth) (lower panel) during cruises M136 &
1217 M137 and M92 along the 12° S transect.

1218 Fig. 3: Near-bottom water concentrations of dissolved Fe and Cd and dissolved Fe to
1219 silicic acid ratios 0.5 m to 4 m above the seafloor across the 12° S transect. The red
1220 diamonds show results from a second sampling at Station 1 one month later.
1221 Concentrations of silicic acid are listed in Table S3 in the supplement.

1222 Fig. 4: Pore water dissolved Fe(II) and hydrogen sulfide concentrations. Data from
1223 an earlier cruise, M92, at Station 1 (75 m water depth) are displayed for comparison.
1224 The uppermost sample represents the bottom water concentration. The analytical
1225 error is smaller than the symbol size.

1226 Fig. 5: Dissolved Fe concentrations in incubated bottom waters from benthic chamber
1227 incubations. The black dashed line represents the linear regressions of the
1228 concentration change over the incubation time. The equations for these linear
1229 regressions are listed together with the coefficients of determination (R^2) in Table S4
1230 in the supplement. The grey dashed line represents theoretical concentration
1231 gradients over the incubation time based on our benthic diffusive fluxes (Table 2).
1232 The analytical error is smaller than the symbol size.

1233 Fig. 6: Pore water dissolved Cd and hydrogen sulfide concentrations. The uppermost
1234 sample represents the bottom water concentrations. The analytical error is smaller
1235 than the symbol size.

1236 Fig. 7: Dissolved Cd concentrations in incubated bottom waters from benthic
1237 chamber incubations. The black dashed line represents the linear regressions of the
1238 concentration change over the incubation time. The equations for these linear

1239 regressions are listed together with the coefficients of determination (R^2) in Table S4
1240 in the supplement. The grey dashed line represents theoretical concentration
1241 gradients over the incubation time based on our benthic diffusive fluxes (Table 3).
1242 The analytical error is smaller than the symbol size.

1243 Fig. 8: Dissolved Fe, nitrate and nitrite concentrations in incubated bottom waters
1244 from the benthic chamber incubation at Station 4 (145 m water depth).

1245 Fig. 9: Comparison of benthic diffusive Fe(II) fluxes between cruises M136 & M137
1246 and M92 on the Peruvian shelf. Negative values represent fluxes from the sediment
1247 pore water into the bottom waters. Shaded bars on the upper panel display the
1248 geochemical conditions in the water column during the time of sampling.

1249 Fig. 10: Schematic overview of the possible mobility of different trace metal to an
1250 expansion of sulfidic conditions. Saturation indices (SI) were calculated for different
1251 H_2S concentrations and reported minimum and maximum concentrations of trace
1252 metals in the water column (data from Bruland and Lohan 2003). Equilibrium
1253 constants ($\log K$ under standard conditions) for Fe (FeS ppt: -3.92), Ni (millerite: -
1254 8.04), Zn (sphalerite: -11.62) and Cd (greenokite: -15.93) were taken from the
1255 PHREEQC WATEQ4F database (Ball and Nordstrom, 1991). The results are
1256 approximate since concentrations instead of activities were used for calculations. A
1257 positive SI is indicative of oversaturation whereas a negative SI is indicative of
1258 undersaturation.

1259 Table 1: Accuracy of replicate concentration measurements (n = 7) of certified
 1260 reference seawater for trace metals NASS-7 and CASS-6 by ICP-MS.

	NASS-7 certified value	NASS-7 measured value	CASS-6 certified value	CASS-6 measured value
Fe (µg/L)	0.351 ± 0.026	0.352 ± 0.017	1.56 ± 0.12	1.56 ± 0.03
Cd (µg/L)	0.0161 ± 0.0016	0.0162 ± 0.0024	0.0217 ± 0.0018	0.0216 ± 0.0016

1261

1262

1263 Table 2: Comparison of benthic diffusive Fe(II) fluxes out of the sediment and
 1264 geochemical bottom water conditions between M136 & M137 and M92 on the
 1265 Peruvian shelf. Fluxes during M92 correspond to similar depth (see Fig. 9).

station	M136 & M137	M136 & M137	M136 & M137	M136 & M137	M136 & M137	M136 & M137	M92	M92
	water depth	latitude	longitude	water column condition	Fe(II) flux diffusive	Fe flux benthic chamber	water column condition	Fe(II) flux diffusive
	(m)	(S)	(W)		(mmol m ⁻² y ⁻¹)	(mmol m ⁻² y ⁻¹)		(mmol m ⁻² y ⁻¹)
1	75	12°13.52	77°10.93	O ₂ < 5 µM	-2.56	–	slightly sulfidic	-22.69
3	130	12°16.68	77°14.95	nitrogenous	-0.81	–	slightly sulfidic	-3.16
4	145	12°18.71	77°17.80	nitrogenous	-17.45	-8.57 ± 2.18	nitrogenous	-5.77
5	195	12°21.50	77°21.70	nitrogenous	-2.49	–	nitrogenous	-1.51
6	245	12°23.30	77°24.82	nitrogenous	-7.96	-5.43 ± 2.36	nitrogenous	-10.20
9	750	12°31.35	77°35.01	O ₂ > 5 µM	0.00	-6.11 ± 3.12	O ₂ > 5 µM	0.00
10	950	12°34.90	77°40.32	O ₂ > 5 µM	-0.26	–	O ₂ > 5 µM	-0.12

1266

1267

1268

1269

1270 Table 3: Comparison of sedimentary Cd excess compared to the lithogenic
 1271 background and the contribution of Cd delivery to the sediment via different
 1272 pathways: (1) diffusion across the sediment-water interface and Cd sulfide
 1273 precipitation within the sediment; (2) Cd incorporation by phytoplankton and delivery
 1274 to the sediment with organic matter; (3) Cd sulfide precipitation in the water column
 1275 and particulate delivery to the sediment.

station	water depth (m)	Cd excess sediment ¹ ($\mu\text{mol m}^{-2} \text{y}^{-1}$)	(1) Cd flux diffusive ($\mu\text{mol m}^{-2} \text{y}^{-1}$)	Cd flux benthic chamber ($\mu\text{mol m}^{-2} \text{y}^{-1}$)	H ₂ S in surface sediment below benthic chamber (μM)	(2) Cd from organic matter ² ($\mu\text{mol m}^{-2} \text{y}^{-1}$)	(3) CdS precipitation in water column ³ ($\mu\text{mol m}^{-2} \text{y}^{-1}$)
1	75	248.87	-1.85	– (3109.5) ⁴	641.02	8.34 – 49.04	199.83 – 240.53
3	130	153.41	0.83	–	–	4.87 – 17.40	135.19 – 147.72
4	145	35.07	0.54	13.4 ± 1.05	1.30	1.55 – 6.48	28.07 – 32.99
5	195	44.76	0.63	22.6 ± 3.24	9.52	5.71 – 7.71	36.36 – 38.36
6	245	35.15	0.55	21.2 ± 3.31	0.40	3.60 – 6.54	28.06 – 31.00
9	750	4.44	-0.30	0.00 ± 0.02	0.00	1.48 – 3.21	1.23 – 2.96
10	950	–	–	–	0.00	–	–

1276

1277 ¹ Calculated after Brumsack (2006) and multiplied by the mass accumulation rate for
 1278 each site (Dale et al., 2015b).

1279 ² Determined by multiplication of Cd/C ratio in average phytoplankton (Moore et al.,
 1280 2013) with particulate organic carbon rain rates (maximum values) and organic
 1281 carbon accumulation rates (minimum values) for each individual site (data from Dale
 1282 et al., 2015b).

1283 ³ Remainder of Cd excess in sediment after subtraction of diffusive and minimum and
 1284 maximum organic Cd sources.

1285 ⁴ Flux calculated from the concentration difference between the bottom water (0.5 m)
 1286 and the first sample from the benthic chamber incubation (taken after 0.25 h).

1287

1288

1289 Table 4: Modelled half-lives ($t_{1/2}$) of dissolved Fe within the first 4 m distance from the
 1290 seafloor at Stations 3 and 4 and data used for determination of $t_{1/2}$ using Eq. (4) and
 1291 Eq. (5).

station	water depth (m)	Si(OH) ₄ flux benthic chamber (F_{Si}) ($\mu\text{mol cm}^{-2} \text{d}^{-1}$)	Si(OH) ₄ concentration gradient (d_{Si}) ($\mu\text{mol cm}^{-3} \text{cm}^{-1}$)	eddy diffusion coefficient (K_y) ($\text{m}^2 \text{s}^{-1}$)	modelled Fe at sediment surface (C_{BW}) (nM)	Fe oxidation constant (k_{Feox}) (d^{-1})	half-life in near- bottom water column ($t_{1/2}$) (min)
3	130	0.73	$-4.05 \cdot 10^{-6}$	$1.55 \cdot 10^6$	70	400	2.5
4	145	0.33	$-1.44 \cdot 10^{-6}$	$1.96 \cdot 10^6$	81	3500	0.3

1292